ELSEVIER

Coordination Chemistry Reviews 228 (2002) 19–41

COORDINATION CHEMISTRY REVIEWS

www.elsevier.com/locate/ccr

Annual survey of organometallic metal cluster chemistry for the year 2000

Michael G. Richmond *

Department of Chemistry, University of North Texas, Denton, TX 76203, USA

Received 6 December 2001; accepted 10 December 2001

Contents

Abstract

The synthetic, mechanistic, and structural chemistry of organometallic metal cluster compounds is reviewed for the year 2000.

Keywords: Organometallic metal cluster compounds

1. Dissertations

The reactivity of $Fe(PF_3)_x(CO)_{5-x}$ under photochemical conditions has been studied. A green volatile iron cluster having the composition $Fe_3(PF_3)_x(CO)_{12-x}$ was observed as the major product [1]. The kinetics and mechanism of the oxidative addition of HER_3 ligands (where E = Si, Ge, Sn; R = various alkyl groups, phenyl) with $H_2Os_3(CO)_{10}$ were examined. The data obtained from the cluster reactions are compared with the literature results for the kinetics and mechanism for the same ligands and their reaction with $Ir(CO)(H)(PPh_3)_2$. HER_3 is proposed to add to $H_2Os_3(CO)_{10}$ via a concerted process and at a single osmium center. The role of the metal cluster in stabilizing the site of unsaturation is discussed. The ligand substitution chemistry and the electrochemical behavior of the orthometalated clusters $HRu_3(C_7H_6NO_2)(CO)_{10}$ and $H_2Ru_3(C_7H_6NO_2)(CO)_8$ have also been investigated [2]. The effect of phosphine ligand substitution on the structures, reactivities, and ligand rearrangements in triosmium clusters has been studied. The isomer preference in $HOs_3(CO)_9(PR_3)(\mu,\eta^2\text{-}CH{=}CH_2)$ has been evaluated as a function of the phosphine ligand. Increasing the size of the PR_3 ligand affords an isomer that bears a vinyl group that is remote to the PR_3 ligand

* Tel.: +1-940-565-3548; fax: +1-940-565-4318.
E-mail address: cobalt@unt.edu (M.G. Richmond).

0010-8545/02/$ - see front matter
PII: S0010-8545(02)00002-4

Nomenclature

ampy	2-amino-6-methylpyridine
bpy	2,2′-bipyridine
bzim	1-benzylimidazole
COD	1,5-cyclooctadiene
Cp	cyclopentadienyl
Cp*	pentamethylcyclopentadienyl
Cy	cyclohexyl
dba	dibenzylideneacetone
bdpp	bis(diphenylphosphino)pentane
depe	bis(diethylphosphino)ethane
dmpm	bis(dimethylphosphino)methane
dpmp	$(Ph_2PCH_2)_2PPh$
dppa	1,2-bis(diphenylphosphino)acetylene
dppb	1,4-bis(diphenylphosphino)butane
dppe	1,2-bis(diphenylphosphino)ethane
dppf	1,1′-bis(diphenylphosphino)ferrocene
dppip	bis(diphenylphosphino)isopropane
dppm	bis(diphenylphosphino)methane
dppp	1,3-bis(diphenylphosphino)propane
dppr	1,1′-bis(diphenylphosphino)ruthenocene
Fc	ferrocenyl
MAS	magic angle spinning
MeCp	methylcyclopentadienyl
nbd	norbornadiene
PPN	bis(triphenylphosphine)iminium
py	pyridine
tpa	tris(2-pyridylmethyl)amine
Tol	tolyl

as the major product. Treatment of $H_2Os_3(CO)_9P$ with ethereal diazomethane gives the methyl/methylene tautomeric pair of clusters $HOs_3(CO)_9P(\mu\text{-Me})/H_2Os_3(CO)_9P(\mu\text{-}CH_2)$. The X-ray structure of $H_2Os_3(CO)_9(PPh_3)(\mu\text{-}CH_2)$ was solved and its molecular structure has been discussed relative to other Os_3 derivatives. The polymerization of diazomethane using $H_2Os_3(CO)_9P$ clusters was also studied [3].

The redox properties of platinum-linked metallophosphine clusters have been investigated as extended one-dimensional cluster arrays. Treatment of the functionalized $Fe_3(CO)_9(\mu_3\text{-PY})(\mu_3\text{-PSnMe}_3)$ (where Y = alkyl or ML_n) clusters with *trans*-$PtI_2(CNC_6H_4\text{–OMe-4})_2$ yields either mono- or bis-platinum clusters depending upon the reaction stoichiometry [4]. The electronic structure of the clusters $Fe_3(CO)_9(\mu_3\text{-EML}_n)_2$ (where E = P, As; ML_n = various metal carbonyl fragments) has been explored by using electronic and vibrational spectroscopies. Fenske–Hall MO calculations have verified the orbital composition of the HOMO → LUMO transition observed in each cluster [5]. Experimental and theoretical studies on the two-electron redox behavior found in $Fe_3(CO)_9(\mu_3\text{-EML}_n)_2$ have been conducted. Fe_3–E_2 bonding in $Fe_3(CO)_9(\mu_3\text{-EML}_n)_2$ has been examined by Fenke–Hall MO calculations. Changes in cluster core bonding may be explained by considering the electronic properties of the ancillary ML_n groups. A Walsh analysis on the orbitals involved in the transformation of the closed 48-electron to the 50-electron form of these clusters has been carried out. The role of the intermediate 49-electron clusters $[Fe_3(CO)_9(\mu_3\text{-EML}_n)_2]^{-\bullet}$ in the structural rearrangements is discussed [6].

The ability of $[Ni_3(dppm)_3(\mu_3\text{-I})(\mu_3\text{-CNR})]^+$ to function as an electrocatalyst for the reduction of CO_2 to CO and carbonate is described [7]. Approaches to organometallic-fused heterocycles employing $[Cp^*RuCl]_4$ have been discussed [8]. Several model cuboidal and cubane clusters have been synthesized and examined for their electron-transfer properties. The new clusters have the form $[(OC)_3MFe_3S_4(SR)_3]^{3-}$ [9].

The polynuclear compounds $Pt_2M_4(C{\equiv}C^tBu)_8$ (where M = coinage metals) were found to be active in hydrocarbon reforming reactions and exhibit high selectivity for light hydrocarbon production. The Pt_2Au_4 cluster revealed greatly enhanced resistance to deactivation processes, unlike the Pt_2Ag_4 and Pt_2Cu_4 systems [10].

The synthesis of $Ir_4(CO)_{12}$ and $Rh_6(CO)_{16}$ using γ-Al_2O_3 is described. The surface-bound species have been characterized and the catalytic reactivity of these clusters as a function of CO removal has been investigated. The use of ^{129}Xe NMR measurements in the study of Rh_6 and Ir_4 clusters in and with the cages of faujasite Y is reported. The NMR data provide valuable evidence for the existence of encaged metal clusters [11].

2. Homometallic clusters

2.1. Group 5 clusters

DFT calculations have been carried out on $[CpTiN]_4$ and the energies and electronic structures of the cubane and planar forms of this cluster examined. Also presented are data from MO calculations on $[CpV(\mu_3\text{-}X)]_4$ (where X = N, P, As). Metal core distortions in these pnicogen-capped clusters are discussed relative to metal–metal bonding interactions [12].

2.2. Group 6 clusters

Hydrolysis of Cp^*MoMe_4 affords the trinuclear cluster $Cp^*_3Mo_3(\mu\text{-}O)_2(\mu\text{-}CH_2)(\mu_3\text{-}CH)$. The presence of the bridging oxo, methylene, and methylidyne groups was established by spectroscopic methods and X-ray crystallography. The utility of $Cp^*_3Mo_3(\mu\text{-}O)_2(\mu\text{-}CH_2)(\mu_3\text{-}CH)$ to function as a model cluster for catalysis on metal oxide surfaces is discussed [13]. Thermolysis of the arsenidene complex $Cp^*As[W(CO)_5]_2$ yields mono- and dinuclear compounds, along with the polynuclear compounds $[W(CO)_3Cp^*W]_2(\mu_3\text{-}As)_4$ and $[W(CO)_3Cp^*W]_2(\mu_3\text{-}As)_3[\mu_3\text{-}AsW(CO)_5]$. Reaction pathways involved in product formation and the X-ray structures of the W_4 and W_5 (Fig. 1) clusters are presented [14].

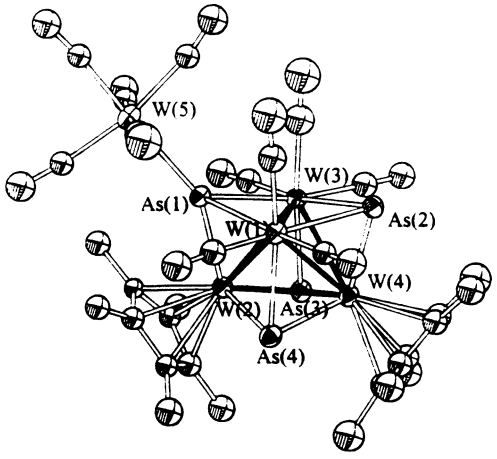

Fig. 1. X-ray structure of $[W(CO)_3Cp^*W]_2(\mu_3\text{-}As)_3[\mu_3\text{-}AsW(CO)_5]$. Reprinted with permission from Organometallics. Copyright 2000 American Chemical Society.

2.3. Group 7 clusters

$Re_3(CO)_{10}(MeCN)_2(\mu\text{-}H)_3$ reacts with 2-vinyltetrahydrothiophene at room temperature to give $Re_3(CO)_{10}(\mu\text{-}H)_3[\mu\text{-}S(CH_2)_3CHCH{=}CH_2]$ and $Re_3(CO)_9(\mu\text{-}H)_3[\mu\text{-}\eta^3\text{-}S(CH_2)_3CHCHCH_2]$. The former product exists in solution as a mixture of equilibrating isomers, one of which has been characterized by X-ray analysis. The interconversion between the isomeric clusters has been examined by 2D EXSYS ^1H-NMR spectroscopy, and the exchange pathways discussed. The solid-state structure of one of the $Re_3(CO)_9$ isomers has been solved by X-ray crystallography [15]. A report demonstrating the formation of $Re_2(CO)_{10}$ from silica-supported $[Re(CO)_3(OH)]_4$ has appeared. The reaction only occurs in the solid state, suggesting that the silica surface plays an important role in this transformation. It is shown that silica-supported $Re_2(CO)_{10}$ can be reoxidized to $[Re(CO)_3(OH)]_4$ on the silica surface at 150–200 °C under nitrogen. The use of XPS measurements and X-ray diffraction structures in the study of these reactions is discussed [16]. The chemistry of $[Re_7C(CO)_{21}]^{3-}$ with $Hg(OAc)_2$ has been investigated, and depending upon the reaction conditions, both $[Re_7C(CO)_{21}(HgOAc)]^{2-}$ and $[Re_6C(CO)_{18}(HgOAc)_2]^{2-}$ may be isolated. The bis-mercury capped cluster reacts with various thiols (HSR) to afford the thiolate-substituted clusters $[Re_6C(CO)_{18}(HgSR)_2]^{2-}$. All new compounds have been characterized in solution by IR and NMR spectroscopy. Included in this report are four X-ray structures (Fig. 2) [17].

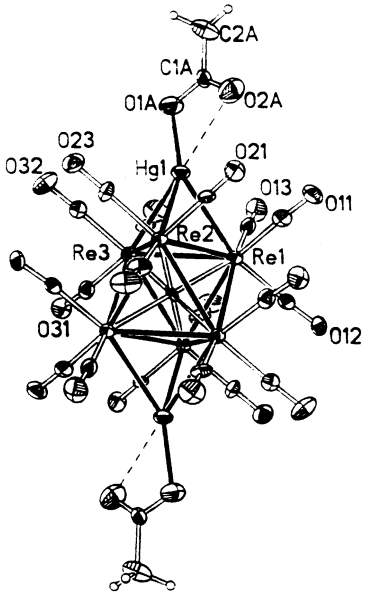

Fig. 2. X-ray structure of $[Re_6C(CO)_{18}(HgOAc)_2]^{2-}$. Reprinted with permission from Inorganic Chemistry. Copyright 2000 American Chemical Society.

2.4. Group 8 clusters

Various heteroaromatic compounds react with triorganovinylsilanes in the presence of $Ru_3(CO)_{12}$ to give heteroarylsilanes. The coupling reaction occurs at the β position relative to a carbonyl directing group [18]. The coupling of ketones with alkenes or alkynes and CO using $Ru_3(CO)_{12}$ as a catalyst yields γ-butyrolactones. This represents the first example of a catalytic [2+2+1] cycloaddition reaction. The effect of phosphines, cyclic alkenes, and various alkynes on the course of the reaction is discussed [19]. The $Ru_3(CO)_{12}$/chloride catalyzed carbonylation of nitroarenes to carbamates has been examined with respect to the role played by the counter alkylammonium cation. A working mechanism based on catalytically active species derived from $Ru(CO)_5$ is presented [20]. Solid–gas hydrogenation of 3-hexyne and 1,4-cyclohexadiene using the clusters $Ru_3(CO)_{12}$, $H_4Ru_4(CO)_{12}$, $H_2Ru_4(CO)_{13}$, and $H_2FeRu_3(CO)_{13}$ has been investigated. The observed catalytic activity is discussed relative to the nature of the solid-state support, and the IR data that reveal the nature of the surface-active species are presented [21]. Treatment of $Fe_3(CO)_{12}$ and the carbollide compound $[HNMe_3][nido\text{-}7\text{-}CB_{10}H_{13}]$ affords the mononuclear complex $[Fe(CO)_3(\eta^5\text{-}7\text{-}CB_{10}H_{11}]^-$ [22]. Metal fragment condensation and carbon–carbon bond cleavage have been observed in the reaction between $Fe_3(CO)_{12}$ and internal propargyl alcohols. While a variety of propargyl alcohols affords binuclear ferrole derivatives, the use of $HC_2CH(OH)R$ (where R = H, Ph) in these reactions yields the triiron clusters $Fe_3(CO)_9(\mu\text{-}CO)(L)$, which contain a parallel alkyne ligand. These two clusters were characterized by IR and NMR spectroscopy. The bow-tie clusters $Fe_5(CO)_{14}(C_2R)_2$ were isolated as the major products when the alkynes $RC_2CH_2(OH)$ (where R = Me, Et) were allowed to react with $Fe_3(CO)_{12}$. The solid-state structures of these Fe_5 clusters were established by X-ray crystallography. Possible mechanisms that account for the observed products are presented [23]. The clusters $M_3(CO)_{12}$ (where M = Ru, Os) have been allowed to react with [2.2]parabenzoindenophane and *anti*-[2.2]indenophane to give $Ru_4H(CO)_9(L–H)$ and $Os_4H(CO)_9(L–H)$. X-ray analyses of these new clusters confirm the C–H bond activation that occurs and the facial $\mu_3\text{-}\eta^5\text{:}\eta^2\text{:}\eta^2$ coordination of an indenyl moiety. ^{1}H-COSY-NMR data have allowed for the complete chemical shift assignment for $Ru_4H(CO)_9(\mu_3\text{-}\eta^5\text{:}\eta^2\text{:}\eta^2\text{-}C_{22}H_{19})$ [24].

A report on the intermolecular activation of *n*-alkanes by $(Cp^*Ru)_3(\mu_3\text{-}H)_2(\mu\text{-}H)_3$ has appeared. When alkanes react with this pentahydride at 170 °C, novel trinuclear *closo*-ruthenacyclopentadiene complexes are produced as the major product. Reaction intermediates observed by NMR spectroscopy and X-ray diffraction data are fully discussed [25]. The synthesis of $RuOs_3(CO)_{13}(\mu\text{-}H)_2$ starting from $Os_3(CO)_{10}(\mu\text{-}H)_2$ and $Ru(CO)_4$(ethylene) and the isomerism in $RuOs_3(CO)_{12}(PPh_3)(\mu\text{-}H)_2$ are described. Hydride mobility in the PPh_3-substituted cluster has been confirmed by VT and EXSY NMR experiments [26]. An NMR study of $H(\mu\text{-}H)Os_3(CO)_{11}$ has revealed the presence of three isomers in solution at 183 K. The difference between these isomers rests on the location of the terminal hydride ligand. Proton T_1 measurements have allowed for the determination of the $H_T–H_B$ distances in each isomer. The activation parameters for hydride scrambling in each isomer have been calculated and used in a discussion on the nature of the transition states involved in the exchange processes [27]. The oxidative addition of HX (where X = Cl, Br, I) to $H_2Os_3(CO)_{10}$ affords four new clusters having the formula $H(\mu\text{-}H)_2Os_3(CO)_{10}(X)$, which differ in the position occupied by the terminal hydride ligand. The observation that the reaction can take place by base catalysis when NH_3 is present is discussed [28]. The new clusters $Os_3(\mu\text{-}H)(CO)_{10}[\mu\text{-}\eta^1\text{:}\eta^2\text{-}HC_2(SiMe_3)C_2(SiMe_3)]$ and $Os_3(\mu\text{-}CO)(CO)_9(\mu_3\text{-}\eta^2\text{-}Me_3SiC_2C_2SiMe_3)$ have been obtained in good yield from the reaction between $Os_3H_2(CO)_{10}$ and the diyne $Me_3SiC_2C_2SiMe_3$. The reaction chemistry of these clusters and the X-ray structures of three compounds are presented [29]. The kinetics and mechanism of HER_3 (where E = Si, R = Et; E = Ge, Sn, R = Bu; E = Sn, R = Ph) addition to $H_2Os_3(CO)_{10}$ have been investigated. $H_3Os_3(CO)_{10}(ER_3)$ is initially formed in these reactions, and in the case of $HSiEt_3$ the reaction is reversible, with a K_{eq} of 100 M^{-1} at 303 K. The rate law is first-order in HER_3 and cluster. Rate comparisons within the HER_3 compounds and with mononuclear 16-electron Ir(I) complexes are discussed [30]. Replacement of the hydroxyl ligand in $Os_3(CO)_{10}(\mu\text{-}H)(\mu\text{-}OH)$ by siloxy ligands occurs readily and furnishes $Os_3(CO)_{10}(\mu\text{-}H)(\mu\text{-}OSiR_2R')$. These clusters have been examined as springboard models to better understand the reactivity of osmium carbonyls on silica surfaces. The X-ray crystal structures of $Os_3(CO)_{10}(\mu\text{-}H)(\mu\text{-}OSiPh_2OH)$ and $Os_3(CO)_{10}(\mu\text{-}H)(\mu\text{-}OSiPh_2OSiPh_2OH)$ have been determined and are discussed relative to model compounds that bear surface geminal and vicinal silanol groups [31]. The mobility of $Ru_3(CO)_6(\mu\text{-}CO)(\mu_3\text{-}\eta^2\text{:}\eta^3\text{:}\eta^5$-acenaphthylene) physisorbed on SiO_2 has been verified by ^{13}C-MAS spectroscopy. The observed molecular reorientational motion was also studied by carrying our T_1 measurements on the CO groups [32]. Trialkylsilanes react with $(\mu_3\text{-}\eta^2\text{:}\eta^3\text{:}\eta^5$-acenaphthylene)$Ru_3(CO)_7$ to furnish $(\mu_3\text{-}\eta^2\text{:}\eta^3\text{:}\eta^5$-acenaphthylene)$Ru_3(H)(SiR_3)(CO)_6$ in good yields. The new clusters were characterized in solution and by X-ray crystallography (Fig. 3). The hydrosilation of alkenes, alkynes, ketones, and aldehydes using the parent cluster was investigated. Ring-opening polymerization of cyclic

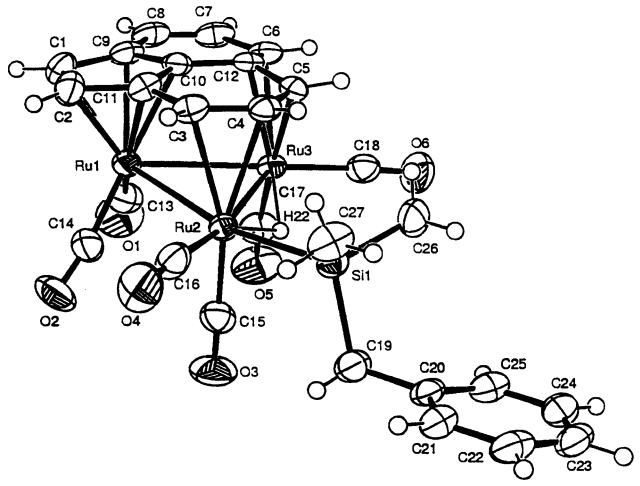

Fig. 3. X-ray structure of (μ_3-η^2:η^3:η^5-acenaphthylene)$Ru_3(H)(SiMe_2CH_2Ph)(CO)_6$. Reprinted with permission from Organometallics. Copyright 2000 American Chemical Society.

ethers with R_3SiH is observed when (μ_3-η^2:η^3:η^5-acenaphthylene)$Ru_3(CO)_7$ is employed as a catalyst [33].

The reaction chemistry of Ru_3 clusters containing allenylidene ligands has been investigated. Treatment of $Ru_3(\mu\text{-}H)[\mu_3\text{-}C_2CAr_2(OH)](CO)_9$ (where Ar = Ph, 4-MeC_6H_4) with HBF_4 affords $Ru_3(\mu\text{-}H)(\mu_3\text{-}CCCAr_2)(CO)_9$. The ligand substitution chemistry with PPh_3 and the data from six X-ray structures are discussed [34]. The oxidative addition of azulene to $Os_3(CO)_{11}(MeCN)$ furnishes $Os_3(\mu\text{-}H)_2(CO)_9(\mu_3\text{-}\eta^1\text{:}\eta^1\text{:}\eta^1\text{-}C_{10}H_6)$ in high yield. The polyene ligand is bound perpendicularly to the Os_3 plane and functions as a four-electron donor ligand forming one terminal and one bridging carbene–osmium bond. The X-ray structure and NMR data (^1H–^{13}C HMQC and ^{13}C EXSY) have been employed in the determination of the solid-state structure and CO exchange behavior, respectively [35]. Norbornene has been allowed to react with $Os_3(CO)_{10}(MeCN)_2$ to give two isomeric clusters having the formula $Os_3(\mu\text{-}H)(CO)_{10}(\mu\text{-}\eta^1\text{:}\eta^2\text{-}C_7H_9)$ and the dihydride complex $Os_3(\mu\text{-}H)_2(CO)_9(\mu\text{-}\eta^1\text{:}\eta^2\text{:}\eta^1\text{-}C_7H_8)$. The X-ray structures of all three products have been solved, and the thermolysis chemistry, which ultimately converts the isomeric hydride clusters into the dihydride cluster, has been outlined. The use of these clusters as models for organic substrate chemisorption and reactivity on metal surfaces is discussed relative to the bonding mode exhibited by the polyene ligand [36]. Several new μ_3-(‖) hydroxyalkyne clusters $Ru_3(CO)_9(\mu\text{-}CO)[\mu_3\text{-}C(H)=CC(R)OH(R')]$ have been prepared and examined for their acid-promoted reactivity. In the presence of alumina, these clusters react to give $Ru_3(CO)_9(\mu\text{-}H)[\mu_3\text{-}C_2C(R)OH(R')]$; the same products are also obtained during thermolysis reactions. The pentaruthenium clusters $Ru_5(CO)_{15}(\mu_4\text{-}C=C=CPh_2)$ and $Ru_5(CO)_{15}[\mu_5\text{-}C=C=C(Ph)Me]$ have been isolated from the requisite propargyl alcohol in the presence of acid. These Ru_5 clusters are shown to contain unprecedented multi-site bound allenylidene ligands and unusual ruthenium atom arrangements, as revealed by X-ray analysis [37]. The acetylide-bound cluster $Ru_3(CO)_8(MeCN)(\mu\text{-}H)(\mu\text{-}C_2^tBu)$ reacts with terminal alkynes and alkynols to give clusters derived from the addition of three molecules of alkyne/alkynol. The reaction chemistry and results of the solution characterization are fully described. The X-ray structures of the butadienyl cluster $Ru_3(CO)_8[\mu_3\text{-}\eta^8\text{-}C(^tBu)=CC(Ph)=C(H)Ph]$ and $Ru_3(CO)_5(\mu\text{-}CO)[\mu_3\text{-}\eta^5\text{-}CC(^tBu)OC(Ph)_2CCH][\mu_3\text{-}\eta^6\text{-}CHC(CPh_2OH)COC(CPh_2)CH]$ have been solved and their structures discussed [38].

The photochemical reactivity of $Os_3(CO)_{10}$(diene) under near-UV irradiation has been investigated. Nanosecond time-resolved infrared and UV–vis spectroscopic evidence for the direct observation of an open Os_3 triangle as the primary photoproduct is presented. Fragmentation of this photoproduct gives $Os(CO)_3$(diene) and $Os_2(CO)_7$ [39]. 1,4-Bis(ferrocenyl)-1,3-butadiyne reacts with $Os_3(CO)_{11}(MeCN)$ in refluxing hexane to produce $Os_3(CO)_{10}(\mu_3\text{-}FcC_4Fc)$ and $Os_3(CO)_{11}(\mu_3\text{-}FcC_4Fc)$. X-ray structural studies reveal that one of the alkyne linkages bridges the Os_3 frame in $Os_3(CO)_{10}(\mu_3\text{-}FcC_4Fc)$ while both alkyne units are coordinated to an open Os_3 triangle in $Os_3(CO)_{11}(\mu_3\text{-}FcC_4Fc)$ (Fig. 4). The extent of electronic communication between the osmium atoms and the ferrocenyl units has been evaluated by differential pulse voltammetry (DPV) [40].

MO calculations have been carried out on $Ru_3(CO)_9(\mu_3\text{-}\eta^2,\eta^2,\eta^2\text{-}C_6H_6)$ and $Ru_3(CO)_9(\mu_3\text{-}\eta^2,\eta^2,\eta^2\text{-}C_{60})$ in order to study the bonding of benzene and buckminsterfullerene to $Ru_3(CO)_9$. The MO data

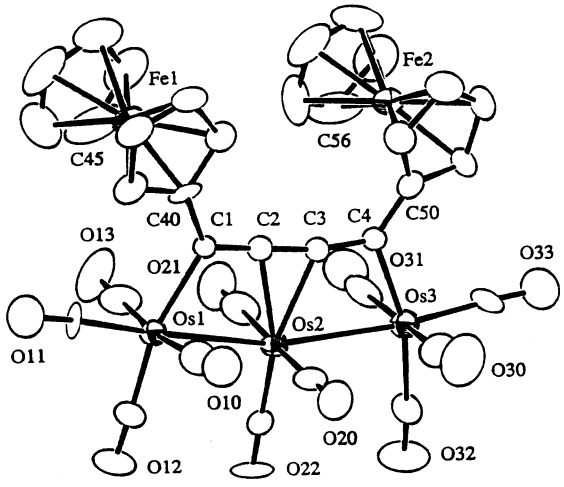

Fig. 4. X-ray structure of $Os_3(CO)_{11}(\mu_3\text{-}FcC_4Fc)$. Reprinted with permission from Organometallics. Copyright 2000 American Chemical Society.

are discussed relative to the carbonyl stretching frequencies and electrochemical properties of the two clusters. The C_{60} polyene ligand binds to the metallic frame by using more of its fragment orbitals than benzene [41]. The synthesis and fluxional NMR behavior of $Ru_3(CO)_9(\mu_3\text{-}\eta^2,\eta^2,\eta^2\text{-}C_{60})$ and $Ru_3(CO)_9(\mu_3\text{-}\eta^2,\eta^2,\eta^2\text{-}C_{70})$ are reported. Thermolysis of these fullerene complexes with PPh_3 leads to PPh_3-substituted derivatives. VT ^{13}C- and ^{31}P-NMR data have been used in the structural characterization of all new clusters [42]. Me_3NO-induced decarbonylation of $Os_3(CO)_9(\mu_3\text{-}\eta^2,\eta^2,\eta^2\text{-}C_{60})$ in the presence of PMe_3 yields $Os_3(CO)_{9-n}(PMe_3)_n(\mu_3\text{-}\eta^2,\eta^2,\eta^2\text{-}C_{60})$ (where $n = 1$–3). The unequivocal identity of the bis- and tris-substituted derivatives has been determined by X-ray methods, and the relationship between the solid-state structure and solution structure, as aided by VT ^{13}C- and ^{31}P-NMR studies, is discussed. The activation barriers for carbonyl exchange are related to the degree of phosphine substitution and the degree of steric hindrance inherent in each cluster [43].

The family of $M_3(CO)_{12}$ (where M = Fe, Ru, Os) clusters has been investigated theoretically by using DFT methods. The optimized geometries are contrasted with known structural data, with agreement being good in the case of the Fe_3 and Ru_3 clusters. Structure predictions for $Ru_2Os(CO)_{12}$ and $RuOs_2(CO)_{12}$, whose X-ray structures are not available, are made, and the D_3 form is found to be more stable than the C_2 form [44]. Data from Fourier-transform ion cyclotron resonance (FTICR) mass spectrometry of $Ru_3(CO)_{12}$ and $Os_3(CO)_{12}$ have been published. The generation of supraclusters and nanoclusters using laser desorption/ionization of discrete metal clusters is discussed, and density functional MO calculations on the electronically unsaturated species $[Ru_3(CO)_6]^-$ are employed in a discussion on the aggregation mechanism [45]. The solvothermal synthesis of $[Fe_6Te_{14}(CO)_{12}]^{2-}$ from $Fe_3(CO)_{12}$ and Na_2Te_2 in H_2O is described. Repeating the same reaction with a small amount of ethanol furnishes $[Fe_4Te_6(TeEt)_2(CO)_8]^{2-}$ as the major product, while use of methanol gives the binuclear complex $[Fe_2Te_3(CO)_6]^{2-}$. The reaction conditions of these high-yield reactions and the molecular structures of all three products are fully discussed [46]. $Os_3(CO)_{12}$ reacts with $[nido\text{-}7\text{-}CB_{10}H_{13}]^-$ in refluxing bromobenzene to give a mixture of the anionic triosmium and monoosmium complexes $[Os_3(CO)_8(\eta^5\text{-}7\text{-}CB_{10}H_{11})]^-$ and $[Os(CO)_3(\eta^5\text{-}7\text{-}CB_{10}H_{11}]^-$, respectively. The reactivity of these complexes towards electrophilic reagents and H^+, along with the effect of the gegencation on the course of the reaction between $Os_3(CO)_{12}$ and the metallacarborane complex, is described [47]. Treatment of $Fe_3(CO)_{12}$ with $Ga_4[C(SiMe_3)_3]_4$ leads to $Fe_3(CO)_9(\mu\text{-}CO)[\mu\text{-}GaC(SiMe_3)_3]_2$, which contains two edges of the Fe_3 triangle bridged by the alkylgallium moieties [48]. The three new clusters $Os_3(CO)_9(\mu_3\text{-}\eta^3\text{-}E\text{-}FcC_3CHFc)(\mu\text{-}H)$, $Os_3(CO)_9(\mu_3\text{-}\eta^3\text{-}Z\text{-}FcC_3CHFc)(\mu\text{-}OH)$, and $Os_3(CO)_9(\mu_3\text{-}\eta^3\text{-}E\text{-}FcC_3CHFc)(\mu\text{-}OH)$ have been prepared from $Os_3(CO)_9(\mu_3\text{-}FcC_4Fc)$ in refluxing THF/H_2O. The molecular structure of each product was ascertained by X-ray crystallography. The redox properties and the extent of electronic communication between the Os_3 core and the ferrocene centers were investigated by DPV measurements [49]. The methanolysis of $Os_3(CO)_{12}$ under Me_3NO activation affords $Os_3(CO)_{10}(\mu\text{-}H)(\mu\text{-}OMe)$ and $Os_3(CO)_{10}(\mu\text{-}OMe)_2$ depending upon the reaction conditions [50]. The reaction between $Fe_2(CO)_9$ and $Cp_2Nb(Te_2H)$ (where Cp = Cp*, C_5Me_4Et) in refluxing toluene affords the triiron clusters $[Fe_3(\mu_2\text{-}H)(\mu_3\text{-}Te)(CO)_9][Cp_2Nb(CO)_2]$ in moderate yields. The X-ray structure of the C_5Me_4Et derivative provides data for the localization of the μ_2-H group in the solid state [51]. The reaction of diphenyl ditelluride with osmium clusters has been explored. $Os_3(CO)_{10}(MeCN)_2$ reacts with Ph_2Te_2 at room temperature to give $Os_3(CO)_{10}(\mu\text{-}TePh)_2$, which possesses an open Os···Os edge that is bridged by one of the TePh units. Thermolysis of this product gives the bis-TePh bridged cluster $Os_3(CO)_9(\mu\text{-}TePh)_2$ initially, followed by production of $Os_3(CO)_9(\mu_3\text{-}TePh)_2$. Treatment of $Os_3(\mu\text{-}H)_2(CO)_{10}$ with Ph_2Te_2 led to a complex mixture of several osmium compounds. Solution spectroscopic data and six X-ray structures are presented and discussed [52].

Two different isomers of $Os_3(\mu\text{-}H)(\mu\text{-}SR)(CO)_9(PCy_2H)$ (where R = Cy, Ph) have been isolated and structurally characterized by X-ray crystallography. The changes in the Os–Os bond distances as a function of the substitution pattern are discussed [53]. Polymeric material having the formula $[Ru_3(CO)_3(SO_2)_2]_n$ has been obtained from the reaction of SO_2 with $Ru_3(CO)_{12}$, $[Ru_3(CO)_{11}Cl]^-$, or $[Ru_3(CO)_{11}]^{2-}$. X-ray diffraction data confirm the amorphous nature of the product polymer [54]. The reactivity of 1,2-ethanedithiol and 1,3-propanedithiol with $Ru_3(CO)_{12}$ and $Os_3(CO)_{10}(MeCN)_2$ has been explored. Whereas $Ru_3(CO)_{12}$ reacts with the former dithiol via fragmentation to give $Ru_2(CO)_6(\mu\text{-}SCH_2CH_2S)$, the major products from the latter dithiol are the compounds $[(\mu\text{-}H)Ru_3(CO)_{10}]_2(\mu\text{-}SCH_2CH_2CH_2S)$ and $Ru_2(CO)_6(\mu\text{-}SCH_2CH_2CH_2S)$. $Os_3(CO)_{10}(MeCN)_2$ reacts with these dithiols to furnish $(\mu\text{-}H)Os_3(CO)_{10}(\mu\text{-}SCH_2CH_2S)$ and $[(\mu\text{-}H)Os_3(CO)_{10}]_2(\mu\text{-}SCH_2CH_2CH_2S)$. The ligand substitution chemistry and thermolysis reactivity of these products have been explored, and the X-ray data from three products are presented and discussed [55]. Treatment of $Os_3(\mu\text{-}H)_2(CO)_{10}$ with $S(allyl)_2$ produces a diastereomeric mixture of $Os_3(\mu\text{-}H)(CO)_{10}[\mu,\eta^2\text{-}(S,C)\text{-}S(allyl)CH_2CH_2CH_3]$ and $Os_3(CO)_{10}[\eta^3\text{-}(S,C,C)\text{-}S(allyl)(CH_2CH{=}CH_2)]$. The crystal and molecular structure of one of the two diastereoisomers has been

established by X-ray crystallography [56]. $Os_3(CO)_{10}(\mu$-dppm) reacts with 1-vinylimidazole at 100 °C to give (μ-H)$Os_3(CO)_7(\mu$-2,3-η^2-[C=NCH=CHN]CH=CH_2) (η^1-[C=NCH=CHN]CH=CH_2) [μ_3-η^3-$PPhCH_2PPh(C_6H_4)$] and $Os_3(CO)_8(\mu$-2,3-η^2-[C=NCH=CHN]CH=CH_2) (η^1-[CH=NCH=CHN]CH=CH_2) (μ_3-η^2-$PPhCH_2PPh_2$). These osmium clusters have been fully characterized in solution by IR and ^{31}P-NMR spectroscopy, and X-ray analysis in the case of the former cluster, which has revealed the bridging hydride, an *N*-coordinated η^1-vinylimidazole group, dimetallated μ,η^2-vinylimidazole moieties, and the fragmentation of the dppm ligand [57]. The disulfurimidophosphinate ligand $(SPPh_2)_2NH$ reacts with $Ru_3(CO)_{12}$ in refluxing THF to afford (μ-H)$Ru_3(\mu_3$-S)[μ_2-S, S, P′-$(SPPh_2)(PPh_2)$N](CO)$_8$ and (μ-H)$Ru_3[\mu_2$-S, S, P′-$(SPPh_2)(PPh_2)$N](CO)$_9$. The solid-state structure of each cluster was established by X-ray analysis [58]. The synthesis of the novel acyl cluster anion $[(\mu_3\text{-Se})Fe_3(CO)_9\{\mu_3\text{-}\eta^1,\eta^1,\eta^3\text{-C(O)CHCCH}_2\}]^-$ and the results of anion functionalization studies have been published. The acyl anion, which was isolated from the reaction between propargyl bromide and $[SFe_3(CO)_9]^{2-}$, has been structurally characterized [59]. Metal–metal and metal–ligand vibrational interactions in the clusters $Fe_3(CO)_9(\mu_3\text{-E})(\mu_3\text{-E}')$ (where E, E′ = S, Se, Te) and low-frequency vibrational spectra of $Co_2Fe(CO)_9(\mu_3$-S) and $Os_3(CO)_9(\mu_3\text{-S})_3$ have been investigated by using infrared and Raman spectroscopy. Detailed assignments are reported, and an attempt to extend to all the modes the plastic cluster model of vibrational analysis is discussed [60]. The labile cluster $Os_3(CO)_{10}(MeCN)_2$ reacts with the thienyl diyne complex $(C_4H_3S)C_2C_2(C_4H_3S)$ to afford the triangular cluster $Os_3(CO)_{10}[\mu_3$-η^2-$(C_4H_3S)C_2C_2(C_4H_3S)]$ and the co-linear cluster $Os_3(CO)_{11}[\mu_3$-η^4-$(C_4H_3S)C_2C_2$-$(C_4H_3S)]$. The X-ray structure of the latter cluster confirms that the diyne moiety is coordinated to the open triosmium frame as a 1,2,3-triene-1,4-diyl unit [61]. Thermolysis of the 2-vinylthiacyclohexane cluster $Os_3(CO)_{10}[\mu$-η^3-$S(CH_2)_4CHCHCH_2]$ produces Os_3-$(CO)_{10}[\mu$-η^4-$S(CH_2)_4CHCHCH_2]$, whose X-ray structure (Fig. 5) reveals an opening of the cluster and a cleavage of one carbon–sulfur bond. This product undergoes further transformations to $Os_3(CO)_{10}[\mu$-$SCH_2CH_2CH_2C(H)=C(H)C(H)=CH_2]$ and $Os_3(CO)_9$-$[\mu$-η^4-*cis*-$S(CH_2)_4CHCHCH_2]$ under thermolysis conditions. This latter cluster is shown to isomerize to $Os_3(CO)_9[\mu$-η^4-*trans*-$S(CH_2)_4CHCHCH_2]$. The course of the thermolysis reaction and the relationship of these clusters to the proposed reaction scheme are discussed [62].

The electronic and steric influences in a series of mono-phosphine-substituted clusters $Os_3(CO)_{11}(PR_3)$ have been studied through the use of X-ray crystallography. Trends involving the Os–Os bond lengths are discussed relative to the properties of the ancillary phosphine ligand [63]. Ionic coupling of $[CpRu(MeCN)_3]^+$ with $H_2Os_3(CO)_{10}(PPh_3)$ yields the tetrahedral cluster $HOs_3(CO)_{10}(PPh_3)(CpRu)$, when DBU is employed as the deprotonation agent. Treatment of $Os_3(CO)_{11}(PPh_3)$ with K/Ph_2CO, followed by the addition of $[CpRu(MeCN)_3]^+$, gives the pentanuclear clusters $Os_3(CO)_{11}(PPh_3)(CpRu)_2$ and $H_2Os_3(CO)_{11}(PPh_3)(CpRu)_2$ and the butterfly cluster $HOs_3(CO)_{11}(PPh_3)(CpRu)$. Carrying out this last reaction with $Os_3(CO)_{11}[P(OMe)_3]$ produces only $Os_3(CO)_{11}[P(OMe)_3](CpRu)_2$, which undergoes orthometallation in refluxing toluene to give the spiked tetrahedral cluster $HOs_3Ru_2(CO)_{11}[P(OMe)_3](\eta^5$-Cp)$(\mu_3$-$\eta^5$-$C_5H_4)$. All new clusters were characterized in solution and by X-ray crystallography in the case of three of the products [64]. The effect of the ancillary phosphine ligand on the methylene/methyl tautomerization in $(\mu\text{-H})_2Os_3(CO)_9P(\mu\text{-CH}_2)$ has been investigated by spectroscopic and kinetic studies. Treatment of (μ-H)$_2Os_3(CO)_9$P with ethereal diazomethane at −78 °C produces a set of clusters with the formula $Os_3(CO)_9P(\text{'}CH_4\text{'})$. When isolated as solids, the methylene tautomers, $(\mu\text{-H})_2Os_3(CO)_9P(\mu\text{-CH}_2)$, are obtained as the preferred species. The X-ray structure of (μ-H)$_2Os_3(CO)_9(PPh_3)(\mu\text{-CH}_2)$ supports this contention. NMR measurements (^{1}H and ^{13}C) reveal that both tautomers are present in solution, with the exact solution structure and tautomer composition being dependent on the P ligand. Rates for tautomer interconversion and the equilibrium constant as a function of the P ligand are reported. Pyrolysis of (μ-H)$_2Os_3(CO)_9(PPh_3)(\mu\text{-CH}_2)$ in toluene gives the methylidyne cluster $(\mu\text{-H})_3Os_3(CO)_8(PPh_3)(\mu\text{-CH})$ in high yield. The reactivity of the different methyl/methylene

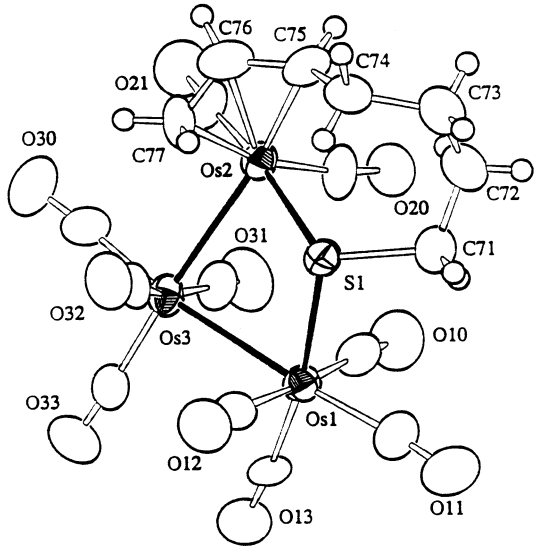

Fig. 5. X-ray structure of $Os_3(CO)_{10}[\mu$-η^4-$S(CH_2)_4CHCHCH_2]$. Reprinted with permission from Organometallics. Copyright 2000 American Chemical Society.

tautomers with ethylene and the ability of these clusters to polymerize diazomethane are described [65]. Treatment of $Ru_3(CO)_{10}(\mu\text{-dppe})$ with 1,3-propanedithiol at 66 °C yields the clusters $(\mu\text{-H})Ru_3(CO)_8[\mu\text{-}S(CH_2)_3SH](\mu\text{-dppe})$ and $Ru_3(CO)_5[\mu_2\text{-}S(CH_2)_3S]_2(\mu^2\text{-dppe})$ in low yields. The molecular structure of each cluster was determined by X-ray methods, and in the case of the latter cluster an open triruthenium frame bearing two doubly bridged propanedithiolate ligands and a chelating dppe ligand was found [66]. The solid-state structure of $Fe_3(CO)_{10}(dppe)$ has been solved, and the dppe ligand is shown to bridge the $Fe(\mu\text{-}CO)_2Fe$ edge of the cluster. The fluxional behavior of the ancillary CO groups exhibits the expected merry-go-round mechanism, and the exchange rates are modulated by the dppe ligand. The NMR results provide data for this first example of a six-toothed failed ratchet process [67]. UV irradiation of the phosphinidene-capped cluster $Fe_3(CO)_9(H)_2(P^tBu)$ in the presence of 1,3-cyclohexadiene affords $Fe_3(CO)_8(\eta^4\text{-}1,3\text{-cyclohexadiene})(\mu_3\text{-}P^tBu)$ as the major product, in addition to minor amounts of $Fe_3(CO)_8(2,5\text{-}\eta\text{-}2,4\text{-hexadiene})(\mu_3\text{-}P^tBu)$ and $Fe_3(CO)_8(1,4\text{-}\eta\text{-}1,3\text{-hexadiene})(\mu_3\text{-}P^tBu)$. These last two clusters arise from the hydrogenolysis of the cyclohexadiene ligand. The unequivocal identity of all three clusters was established by X-ray crystallography. The thermolysis chemistry was examined, and the transformations exhibited by these clusters have been investigated [68]. The coordination chemistry and binding modes of the iminophosphane ligand 2-(diphenylphosphino)-*N*-[2-(diphenylphosphino)benzylidene]benzeneamine (PNCHP) to triosmium clusters have been studied. $Os_3(CO)_{11}(MeCN)$ and $Os_3(CO)_{10}(MeCN)_2$ react with PNCHP to give two coordination isomers of $Os_3(CO)_{11}(PNCHP)$ and 1,1-$Os_3(CO)_{10}(PNCHP)$, respectively. Treatment of this latter cluster with Me_3NO furnishes $Os_3(\mu\text{-H})(CO)_7(\mu_3\text{-PNCP})$ as the major product, along with two geometrical isomers of $Os_3(\mu\text{-H})(CO)_8(\mu_2\text{-PNCP})$. Details from the solution spectroscopic data and three X-ray structures are presented and discussed [69]. The reaction of $[Fe_3(CO)_{11}]_2[Ph_2P(CH_2)_nPPh_2]$ and $[Fe_3(CO)_{11}][Ph_2P(CH_2)_nPPh_2\{Fe(CO)_4\}]$ (where $n = 3$, 4, 6) with cyclohexene episulfide in toluene at 70 °C has been examined. Cluster fragmentation was observed, and the resulting Fe_2S_2 complexes have been isolated and characterized in solution by IR and NMR spectroscopy and by Mössbauer spectroscopy [70]. The open 50-electron cluster $Ru_3(\mu_3\text{-Se})_2(CO)_7[P(C_4H_3S)Ph_2]$ and the 48-electron cluster $Ru_3(\mu_3\text{-Se})(\mu\text{-}PPh_2)(\mu\text{-}C_4H_3S)(CO)_6[P(C_4H_3S)Ph_2]$ have been obtained from the reaction between $Ru_3(CO)_{12}$ and $Ph_2(C_4H_3S)PSe$. The molecular structure of the latter cluster was ascertained by X-ray crystallography [71]. The reaction of $[Os_3(\mu\text{-H})(CO)_{10}(\mu\text{-CO})]^-$ with Ph_2SbCl leads to $Os_3(\mu\text{-H})(\mu\text{-}SbPh_2)(CO)_{10}$, $Os_3(\mu\text{-}SbPh_2)_2(CO)_{10}$, and $[Os_3(\mu\text{-H})(\mu\text{-}SbPh_2)(CO)_{10}]_2$. Three X-ray structures are included in this paper. The results of EXSY NMR experiments, which verify the fluxionality of the Os–Os bonds in these clusters, are thoroughly discussed [72]. The reaction of $(\mu\text{-H})Os_3(CO)_8[Ph_2PCH_2P(Ph)C_6H_4]$ with pyridine-2-thiol at room temperature produces $(\mu\text{-H})Os_3(CO)_8(\mu\text{-pyS})(\mu\text{-dppm})$ and $H(\mu\text{-H})Os_3(CO)_8(\eta^2\text{-pyS})[Ph_2PCH_2P(Ph)C_6H_4]$. The former cluster results from the S–H oxidative addition of the pySH ligand, coupled with the demetallation of the phenyl ring belonging to the dppm ligand, whereas the latter 50-electron cluster derives from the oxidative addition of the pySH ligand and coordination of the thiolate moiety to the cluster frame, followed by the cleavage of one of the Os–Os bonds. When the original reaction was examined at 80 °C instead of room temperature, the new cluster $Os_3(CO)_8(\mu\text{-}\eta^2\text{-pyS})[Ph_2PCH_2P(Ph)C_6H_4]$ and the previous two cluster compounds were isolated as major products. Two X-ray structures accompany this report [73]. The complexation and metallation of the phosphinoiminopyridine ligand $Ph_2P(o\text{-}C_6H_4)CH{=}N(CH_2)_2(o\text{-}C_5H_4N)$ (PNN) at triosmium clusters have been investigated. $Os_3(CO)_{10}(MeCN)_2$ reacts with this multifunctional ligand at ambient temperature to give $Os_3(CO)_{10}[\eta^2\text{-}Ph_2P(o\text{-}C_6H_4)CH{=}N(CH_2)_2(o\text{-}C_5H_4N)]$, which upon thermolysis in refluxing toluene affords $Os_3(CO)_9[\mu\text{-}\eta^3\text{-}Ph_2P(o\text{-}C_6H_4)CH{=}N(CH_2)_2(o\text{-}C_5H_4N)]$, $(\mu\text{-H})Os_3(CO)_8[\mu\text{-}\eta^4\text{-}Ph_2P(o\text{-}C_6H_4)CH{=}NCH_2CH(o\text{-}C_5H_4N)]$, and $(\mu\text{-H})Os_3(CO)_8[\mu\text{-}\eta^4\text{-}Ph_2P(o\text{-}C_6H_4)CH{=}N(CH_2)_2(o\text{-}C_5H_4N)]$. $Os_3(CO)_{12}$ reacts with PNN at elevated temperature to give analogous cluster products, along with the diosmium phosphido complex $Os_2(CO)_5(\mu\text{-}PPh_2)[\mu\text{-}\eta^3\text{-}Ph_2P(o\text{-}C_6H_4)CH{=}N(CH_2)_2(o\text{-}C_5H_4N)]$. The X-ray structures of four products have been solved [74]. The solid–gas hydrogenation of 3-hexyne and 1,4-cyclohexadiene using the catalyst precursors $Ru_3(CO)_9(\mu\text{-H})(PPh_2)$, $Ru_3(CO)_{10}(\mu\text{-H})(PPh_2)$, $Ru_3(CO)_7(PPh_2)(C_6H_4)$, and $Ru_4(CO)_{11}(\mu_4\text{-PPh})(C_6H_4)$ deposited on Pyrex glass, silica, and alumina has been explored. The hydrogenation activity is shown to be dependent on the nature of the cluster, substrate structure, and the solid support. Alumina-supported systems are less reactive than the other supported catalysts [75]. The synthesis and solution characterization of $(\mu\text{-H})_3Ru_3(\mu_3\text{-CY})(CO)_{9-n}(PPh_3)_n$ (where $n = 1$, 3; Y = various groups) have been published. Electrochemical measurements indicate that the Π system associated with the apical substituent does not significantly influence the redox chemistry found in these clusters [76]. Thermolysis of $Ru_3(CO)_{12}$ and $Ir_4(CO)_{12}$ in the presence of the water-soluble phosphine ligand PTA gives $Ru_3(CO)_9(PTA)_3$ and $Ir_4(CO)_7(PTA)_5$. The X-ray diffraction structure of each product has been determined, with comparisons made to related cluster analogues. The details pertaining to cluster stability studies in

deoxygenated solutions and aqueous solubility data are presented [77]. $Os_3(CO)_{11}(MeCN)$ reacts with the triphospholene ligand Ph⌈PPhPPhPCPh=C⌉Ph at room temperature to give $Os_3(CO)_{11}$(1,3-Ph⌈PPhPPhPCPh=C⌉Ph), the bridged-cluster $Os_3(CO)_{10}$(1,3-Ph⌈PPhPPhPCPh=C⌉Ph), and the linked-cluster $[Os_3(CO)_{11}]_2$(1,3-PhPPhPPhPCPh=CPh). When the same ligand is allowed to react with $Os_3(CO)_{10}(MeCN)_2$, the major products are the isomeric clusters $Os_3(CO)_{10}$(1,3-PhPPhPPhPCPh=CPh), which have phenyl groups in different orientations. Thermolysis reactions afford the open cluster $Os_3(CO)_9(\mu_3\text{-}\eta^3\text{-}PhPPhPCPh{=}CPhPPh)$ and $Os_3(CO)_9(\mu_3\text{-}\eta^2\text{-}PhPCPh{=}CPhPPh)$. The transformation pathways between these clusters are discussed, and the structural results of six X-ray structures are fully described [78]. The attachment of $Ru_3(CO)_{12}$ to a generation three dendrimer has been realized and the resulting DAB-*dendr*-G4-$[N(CH_2PPh_2)_2]_{32}[Ru_3(CO)_{11}]_{64}$ complex is discussed relative to electron-transfer chemistry [79].

The coordination of NH_3 to $Os_3(\mu\text{-}H)_2(CO)_{10}$ and the conversion of the amine to an imine upon treatment with aldehydes and ketones are described. The reaction solvent controls the stereochemistry of the imine bound to the osmium frame in $H(\mu\text{-}H)Os_3(CO)_{10}$(imine). The role of intramolecular hydrogen bonding in controlling the stereochemical outcome of ligand coordination is discussed, and the identity of the stereoisomers has been established by ^{15}N and ^{13}C labeling studies and T_1 measurements (^{1}H-NMR) [80]. The photochemical reactivity of $Os_3(CO)_{10}(N{-}N)$ (where N–N = 2-acetylpyridine-*N*-isopropylimine) has been investigated. Optical excitation in the visible region leads to the biradical species $(CO)_4Os^{\bullet}{-}Os(CO)_4{-}Os^{+}(CO)_2(N{-}N^{-\bullet})$ as the initial photoproduct. The reactivity of the biradical was studied by nanosecond time-resolved transient absorption and infrared spectroscopy. The rapid back-reaction that regenerates the parent cluster can be slowed in weakly coordinating solvents such as THF and acetone. When the photolysis reactions are carried out in the presence of alkene traps, the biradical is sufficiently stabilized, promoting the charge separation process that affords the zwitterionic cluster $(CO)_4Os^{-}{-}Os(CO)_4{-}$
Os^{+}(alkene)$(CO)_2(N{-}N)$. Spectroscopic data and photoreaction mechanisms are presented and fully discussed [81]. The *ortho*-metallation of 4-phenylazopyridine and 4,4′-azopyridine at $Os_3(CO)_{10}(MeCN)_2$ has been observed under mild conditions. The resulting clusters $Os_3(\mu\text{-}H)(CO)_{10}(\mu\text{-}NC_5H_3{-}N{=}N{=}C_5H_3N)$ and $Os_3(\mu\text{-}H)(CO)_{10}(\mu\text{-}NC_5H_3{-}N{=}N{=}C_5H_3N)Os_3(\mu\text{-}H)(CO)_{10}$ have been isolated and characterized by solution methods and X-ray crystallography [82]. The synthesis and X-ray structure of bridged Os_3 clusters containing chiral 3-carane-type ligands have been published. Treatment of $(\mu\text{-}H)_2Os_3(CO)_{10}$ with (1*S*,3*S*,6*R*)-3-dimethylaminocarane-4-oxime gives $(\mu\text{-}H)Os_3(CO)_{10}(\mu\text{-}ON{=}CR)$ and Me_2NH, while the reaction between $Os_3(CO)_{11}(MeCN)$ and (1*S*,3*S*,6*R*)-3-mercaptocarane-4-one E-oxime yields the cluster $(\mu\text{-}H)Os_3(CO)_{10}(\mu\text{-}SR)$. This latter cluster reacts with Me_3NO to furnish a diastereomeric mixture of $(\mu\text{-}H)Os_3(CO)_9[\mu,\eta^2\text{-}(S,N)\text{-}R]$ [83]. $Ru_3(CO)_{12}$ reacts with bis(diphenylphosphino)amine in the presence of sodium benzophenone ketyl to give $Ru_3(CO)_{10}[(Ph_2P)_2NH]$ as the major product. Thermolysis of $Ru_3(CO)_{12}$ and $(Ph_2P)_2NH$ in toluene affords the disubstituted product $Ru_3(CO)_8[(Ph_2P)_2NH]_2$. Both clusters have been isolated and characterized in solution and by X-ray crystallography. The $(Ph_2P)_2NH$ ligand is shown to bridge adjacent ruthenium centers in each product; the differences in the P–N bond lengths within each X-ray structure are fully discussed [84]. A paper discussing the conformational constraints and the σ-Π-vinyl interchanges in $\mu_3\text{-}\eta^3$-5,6-dihydroquinoline Os_3 clusters has appeared. The rates of σ-Π-vinyl interchanges in $Os_3(CO)_9[C_9H_6$(5-R, 6-R′)N](μ-H) have been measured by ^{1}H-NMR spectroscopy using $^{187}Os{-}^1H$ satellites as the dynamic probe. The effect of the R and R′ groups on the rates of exchange and the solution structure of each product are discussed [85]. The redox chemistry of the electron-deficient clusters $Os_3(CO)_9[\mu\text{-}\eta^2\text{-}(L{-}H)](\mu\text{-}H)$ (where L–H = various heterocyclic ligands) has been investigated by cyclic voltammetric and controlled potential coulometric measurements. The nature of the radical anion in these clusters was examined by time-resolved infrared spectroelectrochemical methods, and the data revealed that the LUMO of each starting cluster is primarily localized on the heterocyclic ligand [86]. The metallation of 2-methyl-2-thiazoline at an osmium cluster was observed when $Os_3(CO)_{10}(MeCN)_2$ and the thiazoline ligand are allowed to react at room temperature. The isolated cluster, $(\mu\text{-}H)Os_3(CO)_{10}(\mu\text{-}\eta^2\text{-}CH_2⌈C{=}NCH_2CH_2S⌉)$, results from C–H bond activation of the 2-methyl group in the heterocyclic ligand. Thermolysis of this product promotes decarbonylation and formation of the dihydride cluster $(\mu\text{-}H)_2Os_3(CO)_9(\mu\text{-}\eta^2\text{-}CH_2⌈C{=}NCH_2CH_2S⌉)$. The solid-state structure of each product was ascertained by X-ray crystallography [87]. The unsaturated cluster $Os_3(CO)_8[Ph_2PCH_2P(Ph)C_6H_4](\mu\text{-}H)$ reacts with diazomethane to afford $Os_3(CO)_7(\mu_3\text{-}CN_2)(\mu\text{-dppm})(\mu\text{-}H)_2$ and $Os_3(CO)_7(\mu_3\text{-}CCO_2H)(\mu\text{-dppm})(\mu\text{-}H)_3$. Treatment of the former cluster with CO at atmospheric pressure in the presence of H_2O (trace) furnishes the latter cluster as a result of the carboxylation of the μ_3-diazo methylidyne ligand. When $Os_3(CO)_7(\mu_3\text{-}CN_2)(\mu\text{-dppm})(\mu\text{-}H)_2$ is allowed to react with H_2 at elevated temperatures, the major products are found to be $Os_3(CO)_8(\mu\text{-dppm})(\mu\text{-}H)_2$ and $Os_3(CO)_{10}(\mu\text{-dppm})$. Two X-ray structures accompany this report. Schemes illustrating the reactivity pathways exhibited by these clusters are presented [88]. The

clusters $Os_3H(\mu\text{-}H)(HN{=}CPh_2)(CO)_{10}$, $Os_3(\mu\text{-}H)(\mu\text{-}HNCHPh_2)(CO)_{10}$, $Os_3(\mu\text{-}H)(\mu\text{-}HN{-}CHPh_2)(HN{=}CPh_2)(CO)_9$, and $Os_3(\mu\text{-}H)[\eta^2\text{-}HN{=}CPh(C_6H_4)](CO)_{10}$ have been isolated from the reaction of benzophenone imine with $Os_3(\mu\text{-}H)(CO)_{10}$ and $Os_3(CO)_{10}(MeCN)_2$. The three X-ray structures that have been determined support the unusual bonding of terminal imino, bridging amido, and orthometalated imino ligands in these triosmium clusters [89]. Hydroxyamine 7-chloro-4-(hydroxyamino)quinoline reacts with $Os_3(CO)_{10}(MeCN)_2$ to produce $(\mu\text{-}H)Os_3(CO)_{10}(\mu_2\text{-}\eta^1\text{-}O\text{-}C_9H_6N_2Cl)$, which is shown by X-ray diffraction analysis (Fig. 6) to contain a novel $\mu_2\text{-}\eta^1$-O-oximate ligand that bridges adjacent osmium centers by an oxygen atom. This product slowly transforms to $(\mu\text{-}H)Os_3(CO)_{10}(\mu_2\text{-}\eta^2\text{-}ON{-}C_9H_6NCl)$. An aromatic C–H moiety in this product leads to an extremely short intramolecular C–H···O–N hydrogen bond and an intramolecular C–H···O=C hydrogen bond simultaneously. These intramolecular hydrogen bonds provide the driving force for the cluster transformation. Details associated with the X-ray structures of both products are presented [90].

The anionic compound $[(\mu\text{-}SePh)(\mu\text{-}S)\{Fe_2(CO)_6\}_2(\mu_4\text{-}S)]^-$ reacts with $CpFe(CO)_2I$ to produce $(\mu_3\text{-}S)_2Fe_3(CO)_8[Se(Ph)Fe(CO)_2Cp]$, whose solid-state structure was determined by X-ray analysis [91]. The *nido* cluster $[\{Fe_3(CO)_9\}\{\mu\text{-}BiFe(CO)_2Cp''\}_2]$ and $[Bi_4\{\mu_3\text{-}Fe(CO)_3\}_3\{Fe(CO)_2Cp''\}_2]$ (where $Cp'' = C_5H_3\text{-}^tBu_2$) have been obtained from the reaction between $Cp''Fe(CO)_2BiCl_2$ and Collman's reagent. The identity of each product was established by solution methods and X-ray crystallography [92]. The results of density functional theory calculations carried out on the phosphorus monoxide complexes $[CpW(CO)_3]_3PO$, $[Ru_4(CO)_{12}PO]^-$, $[Os_4(CO)_{12}PO]^-$, and $[Ru_5(CO)_{15}PO]^-$ have been published. Strong Π-bonding between the PO ligand and the cluster core is observed, and this interaction is shown to have a significant influence on the PO bond strength and IR frequency of the ν(PO) ligand. Bonding trends and vibrational frequency relationships for the coordinated and free PO ligands are discussed [93]. The theoretical and structural analysis of the unsymmetrical binding of the nonconical PNR_2 ligands in $Ru_4(CO)_{12}(\mu_4\text{-}PNR_2)_2$ has been presented. The X-ray structure of $Ru_4(CO)_{12}(\mu_4\text{-}PNEt_2)_2$ confirms the strong distortion inherent in the octahedral Ru_4P_2 core, in addition to a phosphorus coordination mode that is intermediate between μ_4 and μ_2. The origin of this molecular distortion has been analyzed by carrying out EH and DFT calculations [94]. The tetraruthenium clusters $H_4Ru_4(CO)_{10}[\mu\text{-}1,2\text{-}(R/S,\ R/S)\text{-bdpp}]$ and $H_4Ru_4(CO)_{10}[1,1\text{-}(R/S,\ R/S)\text{-bdpp}]$ have been synthesized and examined as catalysts for the asymmetric hydrogenation of tiglic acid. High hydrogenation rates were observed under mild reaction conditions, with enantiomeric excesses being on the order of 40–46%. Details related to the strong chiral induction, which is controlled by the configuration of the chiral auxiliary, are fully discussed. The X-ray structures of $H_4Ru_4(CO)_{10}[1,\text{-}1,2\text{-}(R,R)\text{-bdpp}]$, $H_4Ru_4(CO)_{10}[1,1\text{-}(R,R)\text{-bdpp}]$ and $H_4Ru_4(CO)_{10}[1,1\text{-}(S,S)\text{-bdpp}]$ accompany this paper, along with a scheme outlining the catalytic cycles for the hydrogenation of tiglic acid [95]. Low-temperature ^{1}H-NMR data on $[H_6Ru_4(benzene)_4]^{2+}$ suggest that this cluster contains a H_2 ligand, which undergoes exchange with the other hydride ligands upon warming. T_1 measurements have allowed for the intramolecular hydride distances to be estimated, and these data have been correlated with the bond distances obtained from the X-ray structure of the Ru_4 cluster. Data from DFT calculations are included in this report [96]. The 1,3-diynes RC_2C_2R (where R = Me, Me_3Si, Ph) react with $H_4Ru_4(CO)_{12}$ in refluxing heptane to give $Ru_4(CO)_{12}[\mu_4\text{-}\eta^1{:}\eta^2{:}\eta^2{:}\eta^1\text{-}(RCH_2C_3R)]$ and $Ru_4(CO)_{12}[\mu_4\text{-}\eta^2{:}\eta^1{:}\eta^1{:}\eta^2\text{-}(RCHC)_2]$ in good yield. The former cluster possesses an allene-1,3-diyl ligand coordinated to the butterfly Ru_4 face in an $\eta^1{:}\eta^2{:}\eta^2{:}\eta^1$ mode, while the latter cluster contains a 1,3-diene-2,3-diyl ligand due to the 1,4-dihydrogenation of the diyne ligand. This latter cluster undergoes CO loss to give $Ru_3(\mu\text{-}H)(CO)_9(\mu_3\text{-}\eta^2{:}\eta^2{:}\eta^1\text{-}RCH_2C_2Ph)$ as a result of 1,1,4-trihydrogenation of the diyne moiety and loss of one ruthenium vertex. Each cluster has been fully characterized in solution and by X-ray diffraction analysis in the case of five clusters [97]. Treatment of $Ru(CO)_4$(ethylene) with $[CpRu(CO)_2]_2(\mu\text{-}C{\equiv}C)]$ (where Cp = Cp, MeCp) produces the air-sensitive clusters

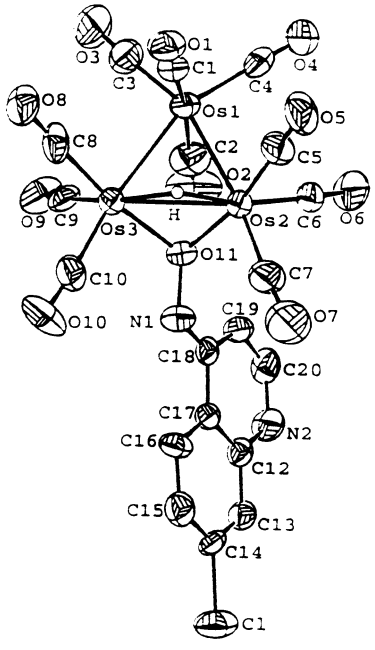

Fig. 6. X-ray structure of $(\mu\text{-}H)Os_3(CO)_{10}(\mu_2\text{-}\eta^1\text{-}O\text{-}C_9H_6N_2Cl)$. Reprinted with permission from Organometallics. Copyright 2000 American Chemical Society.

$Ru_4(\mu_2\text{-}CC)Cp_2(CO)_2(CO)_8$, which contain a permetallated ethene structure. X-ray crystallography has established the solid-state structure of each cluster, and ^{13}C-NMR spectroscopy on ^{13}C labeled $Ru_4(\mu_4\text{-}^{13}C^{13}C)Cp_2(CO)_2(CO)_8$ has allowed for the unequivocal assignment of the carbide carbons [98]. $[Ru_4(CO)_{13}][K]_2$ reacts with $PCl(N^iPr_2)_2$ to give $[Ru_3(CO)_9\{\mu\text{-}P(N^iPr_2)_2\}_3][Ru_6(CO)_{15}(\mu_6\text{-}C)\{\mu\text{-}P(N^iPr_2)_2\}]$. The X-ray structure reveals that the unusual unit cell contains a typical Ru_6 cluster anion with an encapsulated carbide ligand and a 50-electron triruthenium cation. MO calculations on the $Ru_3(CO)_9(\mu\text{-}PR_2)_3$ fragment have been carried out, and these data are compared with other structurally related 48-electron Ru_3 clusters. Predications regarding the redox properties of $Ru_3(\mu\text{-}PR_2)_3$ clusters are included in this report [99]. The synthesis and X-ray structure (Fig. 7) of $[(Cp^*Ru)_3(\mu_3\text{-}S)(\mu_3\text{-}S_2Fc)(\mu_2\text{-}Cl)][FeCl_4]$ have been published. This cluster has been isolated from the reaction of $[Cp^*RuCl]_4$ with 1,2,3-trithia[3]ferrocenephane [100].

The $\mu\text{-}\eta^2,\eta^2$ to $\mu_3\text{-}\eta^2,\eta^2,\eta^2$ interconversion of a C_{60} fullerene attached to an Os_5 cluster has been demonstrated. Treatment of the carbide cluster $Os_5C(CO)_{12}(PPh_3)(MeCN)_2$ with C_{60} in refluxing chlorobenzene yields $Os_5C(CO)_{11}(PPh_3)(\mu_3\text{-}\eta^2,\eta^2,\eta^2\text{-}C_{60})$ and $Os_5C(CO)_{12}(PPh_3)(\mu_3\text{-}\eta^2,\eta^2\text{-}C_{60})$. Heating the former cluster under CO leads to the latter cluster due to CO coordination and a change in the C_{60} bonding mode. The synthesis and X-ray structure of $Ru_5C(CO)_{11}(PPh_3)(\mu_3\text{-}\eta^2,\eta^2,\eta^2\text{-}C_{60})$ are presented, and structural comparisons with the osmium analogue are discussed. The differences observed in the $\mu_3\text{-}\eta^2,\eta^2\text{-}C_{60}$ bonding mode in $Os_5C(CO)_{12}(PPh_3)(\mu_3\text{-}\eta^2,\eta^2\text{-}C_{60})$ and $Os_5C(CO)_{11}(PPh_3)(PhCH_2NC)(\mu_3\text{-}\eta^2,\eta^2\text{-}C_{60})$ are attributed to electronic origins [101]. The butadiynedtyldimetal complexes $Cp^*Fe(CO)_2C{\equiv}C{-}C{\equiv}CMCp^*(CO)_2$ (where M = Fe, Ru) react with Group 8 metal carbonyls to afford $Ru_3(CO)_{10}(\mu_3\text{-}C{-}C{\equiv}C\text{-}\mu\text{-}C)Fe_2Cp^*_2(CO)_3$, $(Cp^*Fe)_4Ru_2(CO)_{13}[\mu_6\text{-}C_8{-}C(=O)]$, and $Fp^{*+}[Cp(CO)_2Ru(\eta^2\text{-}C{\equiv}C){-}(\mu_3\text{-}C{\equiv}C)Fe_3(CO)_9]^-$. Schemes that account for the formation of these products, along with two X-ray structures, are presented and fully discussed [102]. Aqueous HCl reacts with $Ru_5(\mu_3\text{-}C{=}CH_2)(\mu\text{-}SMe)_2(\mu\text{-}PPh_2)_2(CO)_{10}$ to furnish the carbyne cluster $Ru_5(\mu_3\text{-}SMe)(\mu_3\text{-}CMe)(\mu\text{-}Cl)(\mu\text{-}SMe)(\mu\text{-}PPh_2)_2(CO)_9$ as a result of hydrogen addition to the vinylidene ligand and chlorine addition to one of the ruthenium edges. The solid-state structure has been solved by X-ray crystallography, and these results confirm the acetylide-like nature of the C_2 ligand in the starting cluster [103]. The synthesis and characterization of $Fe_2M_3(\mu_4\text{-}E)(\mu_3\text{-}E')(CO)_{17}$ and $Os_3(\mu_3\text{-}S)(\mu_3\text{-}E')(CO)_9$ (where M = Ru, Os; E = S, Se, Te; E′ = Se, Te) have been published. The facile reaction conditions found for the synthesis of these clusters are discussed, and the X-ray structures of three products are presented [104]. The reaction between $[Cp(PPh_3)_2Ru]_2[\mu\text{-}(C{\equiv}C)_n]$ (where $n = 3$, 4) and $Fe_2(CO)_9$ gives the pentanuclear compound $Fe_3[\mu_3\text{-}CC{\equiv}C\{Ru(PPh_3)_2Cp\}]_2(CO)_9$. Reactions of the same ruthenium poly-ynyl compounds with $Co_2(CO)_8$ have also been examined [105]. The phosphorus functionalized clusters $Ru_5(CO)_{15}(\mu_4\text{-}PR)$ (where R = various groups) have been prepared from the thermolysis of $Ru_3(CO)_{12}$ with $Ru_4(CO)_{13}(\mu_4\text{-}PR)$. Treatment of $Ru_5(CO)_{15}(\mu_4\text{-}PNR_2)$ with $HBF_4{\cdot}H_2O$ at room temperature gives $Ru_5(CO)_{15}(\mu_4\text{-}PF)$ in high yield; however, carrying out the same reaction in refluxing CH_2Cl_2 affords the cluster $[Ru_5(CO)_{15}(\mu_4\text{-}PO)]^-$ as the major product. The alkoxy phosphinidene-capped clusters $Ru_5(CO)_{15}(\mu_4\text{-}POR')$ are isolated in good yields when this μ_4-capped phosphorus monoxide cluster is allowed to react with alcohols. The transformations exhibited by these clusters are discussed, and the results of solution spectroscopic characterization are presented. The X-ray structures of six clusters have been solved and the structural differences fully contrasted [106]. A report on the reversible adduct formation between the carbido cluster $Ru_5C(CO)_{15}$ and MeCN has appeared. Stopped-flow kinetic measurements in 1,2-DCE have allowed for the determination of the kinetic parameters associated with this reaction. These data suggest that the attack of MeCN on the cluster occurs via cleavage of a Ru–Ru bond, coupled with an opening of one edge of the cluster. This scheme is supported by a low ΔH^+ value, which is consistent with an early transition state involving ligand attack and polyhedral rearrangement. Kinetic and thermodynamic measurements on the loss of MeCN from the intermediate adduct cluster have been carried out, and these data provide a detailed picture regarding the release of strain within the cluster upon release of the MeCN ligand [107]. UV–vis irradiation of $Ru_5C(CO)_{15}$ in the presence of Et_3SiH

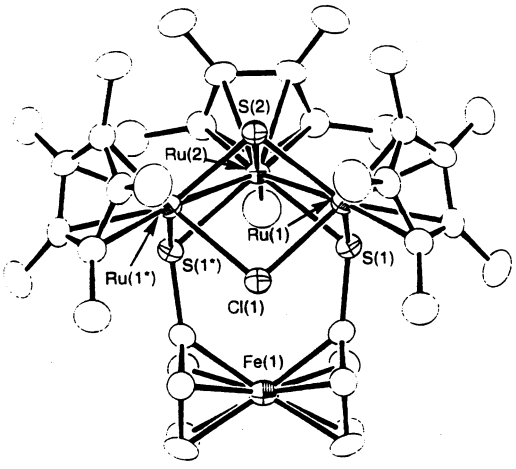

Fig. 7. X-ray structure of $[(Cp^*Ru)_3(\mu_3\text{-}S)(\mu_3\text{-}S_2Fc)(\mu_2\text{-}Cl)]^+$. Reprinted with permission from Organometallics. Copyright 2000 American Chemical Society.

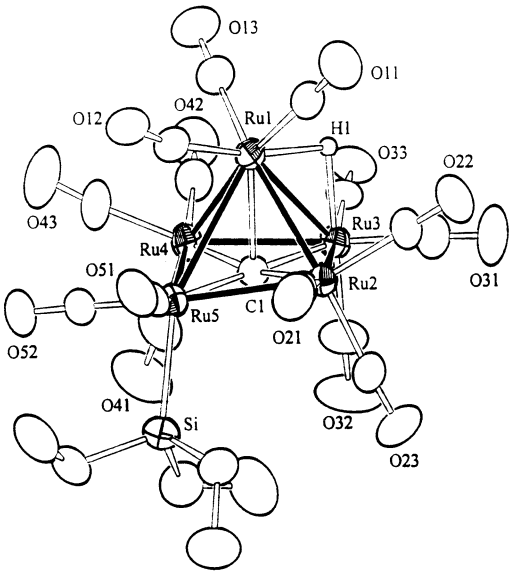

Fig. 8. X-ray structure of $Ru_5(CO)_{14}(SiEt_3)(\mu_5\text{-}C)(\mu\text{-}H)$. Reprinted with permission from Organometallics. Copyright 2000 American Chemical Society.

yields $Ru_5(CO)_{14}(SiEt_3)(\mu_5\text{-}C)(\mu\text{-}H)$ and $Ru_5(CO)_{15}(SiEt_3)(\mu_5\text{-}C)(\mu\text{-}H)$ in low yield. Treatment of the former cluster with CO gives the latter product, while thermolysis of $Ru_5(CO)_{15}(SiEt_3)(\mu_5\text{-}C)(\mu\text{-}H)$ proceeds by CO loss to furnish the corresponding $Ru_5(CO)_{14}$ cluster. Both clusters were structurally characterized by X-ray analysis. A square pyramidal cluster was found for $Ru_5(CO)_{14}(SiEt_3)(\mu_5\text{-}C)(\mu\text{-}H)$ (Fig. 8), where the ancillary $SiEt_3$ moiety is bound to one of the basal ruthenium centers. The butterfly structure observed in $Ru_5(CO)_{15}(SiEt_3)(\mu_5\text{-}C)(\mu\text{-}H)$ contains a hydride bridge across the hinge Ru–Ru bond on the butterfly and a $SiEt_3$ group attached to the bridging ruthenium atom [108].

A report on the applications of laser desorption and electrospray ionization (ESI) mass spectrometry in identifying transition-metal clusters has appeared. Some of the clusters examined include $[Os_{10}C(CO)_{24}]^{2-}$, , $[Os_{20}(CO)_{40}]^{2-}$, and $[Os_{17}(CO)_{36}]^{2-}$ [109]. Thermolysis of $H_3Os_3(CO)_9(BCO)$ yields $H_3Os_6(CO)_{16}B$. This 86-electron cluster exhibits a new Os_6 polyhedral geometry, as judged by X-ray diffraction analysis. The observed structure may be viewed as being derived from a pentagonal bipyramid that is missing one equatorial vertex; alternatively, the cluster geometry may also be viewed as a bicapped tetrahedron, with a boron atom occupying an edge of the tetrahedron that is common to the capped faces. The structure of $H_3Os_6(CO)_{16}B$ is discussed relative to electron counting rules [110]. $Ru_6C(CO)_{17}$ reacts with the alkyne linking reagent $Ph_2PC_2PPh_2$ in refluxing THF to produce the new cluster-based polymer $[Ru_6C(CO)_{15}(Ph_2PC_2PPh_2)]_n$ (where $n \approx 1000$). Irradiation of this polymer in an electron beam yields the first nanoparticle chains, followed by conducting wires. Other products isolated from the THF reaction include $Ru_6C(CO)_{16}(Ph_2PC_2PPh_2)$, $Ru_6C(CO)_{15}(Ph_2PC_2PPh_2)_2$, and $Ru_5C(CO)_{13}(Ph_2PC_2PPh_2)$ [111]. New linked and threaded cluster compounds have been prepared. The reaction of $Ru_6C(CO)_{17}$ with various crown ethers affords clusters having the general formula $Ru_6C(CO)_{14}(\eta^6\text{-crown ether})$. The solution characterization of these clusters and four X-ray structures are discussed [112]. The addition of two equivalents of $SnCl_4$ to $[Ru_6C(CO)_{16}]^{2-}$ furnishes $[Ru_6C(CO)_{16}(SnCl_3)]^-$ initially, followed by the formation of $Ru_6C(CO)_{16}(SnCl_2)$. The latter cluster may also be prepared from the reaction of $Ru_6C(CO)_{17}$ with $SnCl_2$. The X-ray structures of $[Ru_6C(CO)_{16}(SnCl_3)]^-$ and $Ru_6C(CO)_{16}(SnCl_2)$ accompany this report [113]. Insights into the elimination of formaldehyde from $[Ru_6C(CO)_{16}(CO_2Me)]^-$ and $[Rh_6(CO)_{15}(CO_2Me)]^-$ have been revealed through the use of electrospray mass spectrometry. The ancillary CO_2Me group rearranges to form a strong multicenter bonding interaction prior to CO loss and elimination of formaldehyde [114]. The ketenylidene cluster $[Fe_3(CO)_9(CCO)]^{2-}$ reacts with triflic anhydride to give the polycarbon metal cluster $[Fe_6(CO)_{18}C_4]^{2-}$. The existence of the C_4 ligand in $[Fe_6(CO)_{18}C_4]^{2-}$ was verified by X-ray crystallography. The C–C bond lengths of the C_4 ligand in the product closely resembles those in free 1,3-butadiene [115].

2.5. Group 9 clusters

The twenty-one-vertex globular cluster $Cp^*_3Ir_3B_{18}H_{15}(OH)$ has been prepared from *syn*-$B_{18}H_{20}$ and $[Cp^*IrCl_2]_2$ [116]. A report describing the synthesis and magnetic properties of $[Co_2\{O_2CCCo_3(CO)_9\}_5]^-$ has appeared. X-band EPR data and magnetic susceptibility measurements on this cluster reveal that it acts as a two spin $S_1 = S_2 = 3/2$ Heisenberg model. MO calculations have been carried out, and the results were employed in a discussion on the pathways available for magnetic exchange between the two different Co(II) centers [117]. The $Co_3(CO)_9C$ moiety has been utilized as an electroreducible marker for estradiol detection enhancement. The synthesized complex has the general formula $Co_3(CO)_9CC(O)NHC_6H_4C{\equiv}CE$ (where E = estradiol). This compound retains an acceptable relative binding affinity for estradiol receptor, facilitating its use as an electrochemical marker for biochemical analyses [118]. Sodium amalgam reduction of $Co_3(CO)_9(\mu_3\text{-}E)$ (where E = S, Se) leads to $[Co_3(CO)_9(\mu_3\text{-}E)]^-$, which when allowed to react with allyl bromide afford $Co_3(CO)_7(\mu\text{-}\eta^3\text{-allyl})(\mu_3\text{-}E)$. These clusters represent the first examples of cobalt complexes that possess a bridging $\mu\text{-}\eta^3$-allyl ligand. The solid-state structure of the selenium derivative was determined, and the bridging of adjacent

cobalt centers by an equatorially disposed allyl moiety was confirmed [119]. Impure $FcPCl_2$ reacts with $Na[Co(CO)_4]$ in THF to produce $Co_3(CO)_7(\mu_3\text{-PFc})(\mu_2\text{-}PFc_2)$ and $Co_3(CO)_7(\mu_3\text{-PFc})(\mu_2\text{-PHFc})$ in low yields. Both clusters contain 48 valence electrons and have the expected tetrahedral Co_3C skeleton. The X-ray diffraction structures of both clusters were solved, and the redox behavior of these clusters was examined by cyclic voltammetry. The former product cluster exhibits two reduction waves in the CV, while only one reduction wave is observed in the latter cluster. The multiple reduction couples in $Co_3(CO)_7(\mu_3\text{-PFc})(\mu_2\text{-}PFc_2)$ are believed to originate from separate redox sites at different cobalt centers [120]. A study on the regioselective metal exchange reactions in linked clusters has been published. The clusters $[(CO)_9Co_3(\mu_3\text{-}C)CO_2CH_2]_2$ and $(CO)_9Co_3(\mu_3\text{-}C)CO_2CH_2(\mu\text{-}C{\equiv}CH)Co_2(CO)_6$ react with a variety of carbonyl metalate anions to produce new heterometallic tetrahedrane clusters. The X-ray structures of $(CO)_9Co_3(\mu_3\text{-}C)CO_2CH_2CH_2O_2C(\mu_3\text{-}C)Co_2Mo(CO)_8Cp$ and $(CO)_8CpCo_2Mo(\mu_3\text{-}C)CO_2CH_2(\mu\text{-}CCH)Co_2(CO)_6$ have been solved and are discussed relative to other Co_2Mo tetrahedrane clusters [121]. $[Cp^*MCl_2]_2$ (where M = Rh, Ir) react with H_2Se to give $[(Cp^*M)_3(\mu_3\text{-}Se)_2]^{2+}$ (Fig. 9). The dimer $(Cp^*MCl)_2(\mu\text{-}SeH)_2$ is shown to be an intermediate to the trinuclear clusters, as well as several other tetranuclear cluster compounds that possess μ_3-Se ligands. A total of six X-ray structures accompany this report [122].

A report on the intermolecular Pauson–Khand reaction in supercritical ethylene using $Co_4(CO)_{12}$ and $Co_4(CO)_{11}[P(OPh)_3]$ as catalyst precursors has appeared. High conversions and moderate reaction times were observed [123]. $Co_4(CO)_{12}$ serves as a practical catalyst for the Pauson–Khand reaction in the presence of cyclohexylamine. A wide variety of substrates were shown to participate in the cyclization reaction with relatively high yields [124]. The role of added phosphine in controlling the chemoselectivity in the hydroformylation of 4-vinylpyridine using $Rh_4(CO)_{12}$ is discussed. Reactions carried out with $Rh_4(CO)_{12}$ and $Rh_4(CO)_{12}$/PMe_2Ph reveal dramatically different results. The presence of an ancillary phosphine ligand changes the polarization of the alkyl–rhodium bond to such a degree that acyl–rhodium formation becomes favored relative to hydrogenation [125]. Partially decarbonylated tetrairidium clusters on MgO have been prepared, structurally characterized, and examined in toluene hydrogenation reactions. Starting with $Ir_4(CO)_{12}$, the major surface-supported species was found to be $[HIr_4(C\bar{O})_{11}]^-$, which was identified by IR and EXAFS spectroscopies [126]. The use of $Ir_4(CO)_{12}$ and $Ir_6(CO)_{16}$ in the presence of highly dispersed metal catalysts on oxide surfaces and zeolites is described [127]. The homogeneous hydroformylation of ethylene using the catalyst precursor $Rh_4(CO)_{12}$ has been investigated. Intermediates involved in the reaction were assessed by in situ high-pressure infrared spectroscopy. At high CO pressure and autogeneous hydroformylation conditions, the mononuclear acyl rhodium tetracarbonyl is observed, while at low CO pressures a species assigned to $EtRh(CO)_4$ is observed. The spectroscopic data are discussed, and the importance of the reaction conditions on the observed species is stressed [128]. The sol–gel entrapped compounds $Rh_2Co_2(CO)_{12}$, $[FeCo_3(CO)_{12}]^-$, and $[(CO)_4Fe(\mu\text{-}PPh_2)Pd(\mu\text{-}Cl)_2]_2$ have been prepared and examined as alkene isomerization and hydrogenation catalysts. $Rh_2Co_2(CO)_{12}$ is converted into sol–gel trapped carbonyl-free nanoparticles under hydrogenation conditions, and these nanoparticles are shown to be efficient catalysts for the reduction of aromatic C–C bonds [129]. The X-ray structure of $Rh_4(CO)_{12}$ has been redetermined at 293 and 173 K and the thermal motion analyzed relative to the dynamic behavior exhibited by this cluster. There is significant internal motion of the ancillary CO groups relative to the metal skeleton. The motion is in agreement with a normal mode or modes of C_3 symmetry [130]. $Rh_4(CO)_{12}$ dissolves in concentrated H_2SO_4, HSO_3CF_3, and magic acid under CO to give the square-planar Rh(I) species $[Rh(CO)_4]^+$ and H_2. The identity of $[Rh(CO)_4]^+$ was ascertained by vibrational spectroscopies and NMR measurements [131]. Selective ^{59}Co-NMR inversion-recovery measurements on $Co_4(CO)_{12}$ have provided information on the ^{59}Co relaxation process and CO exchange pathways. The quadrupole coupling constant measured in solution complements previous solid-state NMR data. All four cobalt atoms are involved in the CO exchange process, which signal that the CO scrambling is complete. This

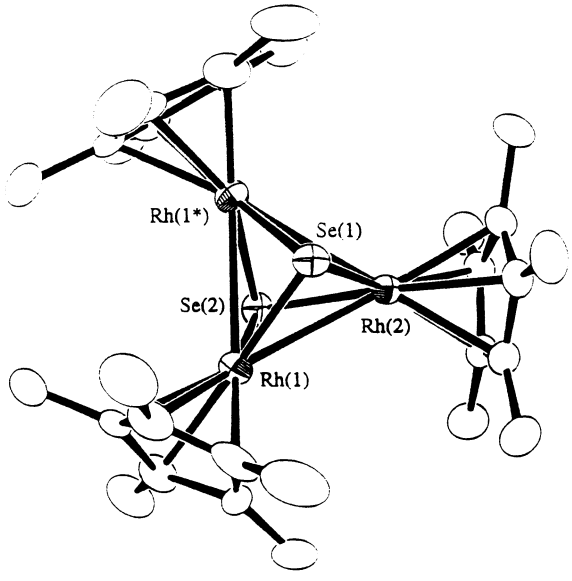

Fig. 9. X-ray structure of $[(Cp^*Rh)_3(\mu_3\text{-}Se)_2]^{2+}$. Reprinted with permission from Organometallics. Copyright 2000 American Chemical Society.

premise is corroborated by 2D-EXSY ^{59}Co-NMR studies. The measured rate constants and the experimentally determined activation parameters are found to be in the range reported for other M_4 clusters [132]. $Ir_4(CO)_{10}[\mu\text{-}(Ph_2P)_2CH_2]$ reacts with dried KOH to give initially $[Ir_4(CO)_{10}\{\mu\text{-}(Ph_2P)_2CH\}]^-$, followed by the formation of $[Ir_4(CO)_9\{\mu_3\text{-}(Ph_2P)_2CH\}]^-$. When the same starting material is allowed to react with DBU or K_2CO_3 in wet CH_2Cl_2 under CO, only the hydrido anion $[HIr_4(CO)_9\{\mu\text{-}(Ph_2P)_2CH\}]^-$ is observed. The X-ray structures of the latter two products are presented, and VT ^{13}C-NMR data for carbonyl scrambling are discussed [133]. 1,2,3-Triphenylphosphirene reacts with $HIr_4(CO)_{10}(\mu\text{-}PPh_2)$ to give $Ir_4(CO)_8(\mu_3\text{-}\eta^2\text{-}PhPCPh{=}CPh)(\mu\text{-}PhPCPh{=}CHPh)(\mu\text{-}PPh_2)$, which is shown by X-ray analysis to contain phosphametallacycle ($\mu_3\text{-}\eta^2$-PhPCPh=CPh) and phosphidoalkenyl (μ-PhPCPh=CHPh) ligands that arise from insertion and hydrometallation processes, respectively. $HIr_4(CO)_9(PPh_3)(\mu\text{-}PPh_2)$ reacts with the same phosphirene to give the CO substitution products $HIr_4(CO)_{9-n}(PPh_3)(\eta^1\text{-}PhPCPh{=}CPh)_n(\mu\text{-}PPh_2)$ (where $n = 1$, 2). Mechanistic schemes that account for the observed reactivity are presented, and four X-ray structures have been determined [134]. Treatment of $Ir_4(CO)_{12}$ with 1,1-bis(diphenylphosphino)ethene and dppa gives $Ir_4(CO)_{12-n}(P{-}P)$ (where $n = 1$, 2) depending on the reaction conditions. These new clusters have been fully characterized in solution by IR and ^{31}P-NMR spectroscopies, and by FAB mass spectrometry. The molecular structure of $Ir_4(CO)_8(dppa)_2$ was determined and the bridging nature of the dppa ligands established [135]. A paper describing the synthesis of iridium clusters that possess an η^1 organic ligand has appeared. Refluxing $[HIr_4(CO)_{11}]^-$ with diphenylacetylene gives $[Ir_4(CO)_{11}(CPh{=}CHPh)]^-$, whose X-ray structure shows an η^1 bound vinyl moiety with *cis* phenyl rings that occupies an axial position on the tetrahedral frame of the cluster. The ^{13}C-NMR data, recorded at low temperature, are in full agreement with the solid-state structure. The anionic cluster $[Ir_6(CO)_{14}(CO_2Me)_2]^{2-}$ has been prepared from $Ir_6(CO)_{16}$ and NaOMe. The two carbomethoxy groups are situated on adjacent metal vertices of the octahedral core, as revealed by X-ray crystallography [136].

$Rh_6(CO)_{16}$ has been successfully employed as a catalyst in the copolymerization of norbornadiene derivatives under water–gas shift conditions. The resulting unsaturated polyketones are obtained in high yields [137]. The decomposition of [PPN][$Rh(CO)_4$] at 200 °C under CO yields the encapsulated phosphido cluster $[Rh_{10}P(CO)_{22}]^{3-}$ and provides the first decomposition evidence of the PPN gegencation. The bicapped square antiprismatic Rh_{10} polyhedron of the product was confirmed by X-ray diffraction analysis. These data help explain the reasons for the observed deactivation of [PPN][$Rh(CO)_4$]-based catalytic systems [138]. The

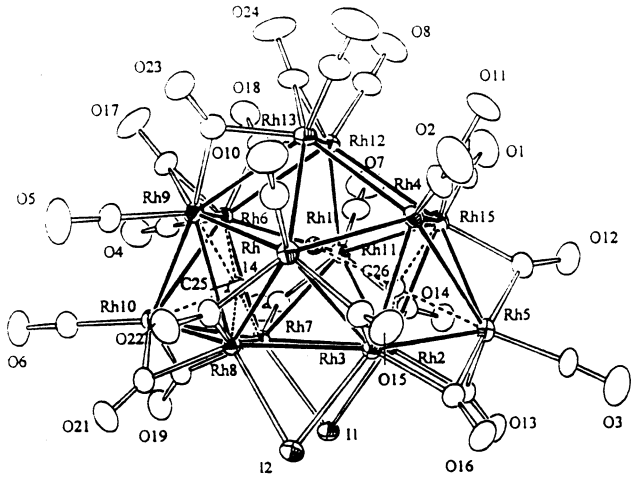

Fig. 10. X-ray structure of $[Rh_{15}C_2(CO)_{24}I_2]^{3-}$. Reprinted with permission from Organometallics. Copyright 2000 American Chemical Society.

reaction of $[Rh_{12}C_2(CO)_{24}]^{2-}$ with different Rh(I) derivatives gives an uncharacterized intermediate that reacts with halides to furnish the cluster anions $[Rh_{15}C_2(CO)_{24}X_2]^{3-}$ (where X = Cl, Br, I). The X-ray structures of the bromo and iodo analogues have been solved (Fig. 10) and found to be isostructural. The $Rh_{15}C_2$ polyhedron is C_{2v} centered and based on a tetracapped pentagonal prism. The disorder in the CO ligands in the bromo cluster is discussed relative to the CO fluxionality observed in solution [139].

2.6. Group 10 clusters

The effect of water on the synthesis of $[Pt_3(CO)_6]_2^{2-}$ from $[Pt(NH_3)_4]^{2+}$ in zeolite matrices has been explored. The rate of carbonylation is affected by the amount of zeolitic water, which assists the migration of Pt species and supplies protons to the charge-compensating species, accelerating the carbonylation reaction. FTIR data are presented and discussed relative to the carbonylation steps [140]. Treatment of $Pt_3(\mu\text{-}CO)_3(PPh_3)_4$ with H_2O_2 affords $Pt_3(\mu\text{-}CO)_3(PPh_3)_3$ in high yields. The reaction between $Pt_3(\mu\text{-}CO)_3(PR_3)_3$ (where R = various groups) and SO_2 leads to CO loss and formation of $Pt_3(\mu\text{-}SO_2)_3(PR_3)_3$ and $Pt_3(\mu\text{-}CO)_2(\mu\text{-}SO_2)(PR_3)_3$. The monocarbonyl derivative may be prepared by allowing $Pt_3(\mu\text{-}SO_2)_3(PR_3)_3$ to react with CO (one equiv.) The ^{13}C-NMR spectra of ^{13}CO enriched complexes were recorded, and detailed spectral assignments were made through the use of simulated ^{13}C-NMR spectra with the help of ^{195}Pt-NMR data [141]. Nickelocene reacts with methyllithium in the presence of 2-butyne to furnish several organonickel compounds. Of these products, the 49-electron cluster $(CpNi)_3$(2-butyne) was isolated and structurally characterized. X-ray

analysis reveals that the 2-butyne ligand is bonded to the three nickel atoms via two σ and one Π bonds [142]. Reduction of nickelocene with metallic sodium in the presence of terminal alkynes leads to (μ_3-hydrido)(μ_3-alkylidyne)Ni_3Cp_3 and (μ_3-alkylidyne)Ni_3Cp_3 clusters. The X-ray structures of (μ_3-H)[μ_3-C$(CH_2)_3$Me]Ni_3Cp_3 and [μ_3-C$(CH_2)_4$Me]Ni_3Cp_3 have been solved and the structural details discussed [143].

The 65-electron tetranuclear cluster Cp_3Ni_4(2-butyne)$_3$ has been isolated from the reaction between nickelocene, methyllithium, and 2-butyne. This cluster has been structurally characterized in solution by EPR analysis and its solid-state structure was crystallographically determined [144]. $[\{(C_6F_5)_2Pt(\mu\text{-}PPh_2)_2Pt(\mu\text{-}Cl)\}_2]^{2-}$ reacts with $AgClO_4$ to afford the neutral tetraplatinum compound $Pt_4(\mu\text{-}PPh_2)_3[\mu_3\text{-}PPh(1,2\text{-}\eta^2\text{-}Ph)\text{-}\kappa^3P](C_6F_5)_4$. This 58-electron cluster displays three Pt–Pt bonds and a 1,2-η^2-Ph(phosphido) platinum interaction. This cluster reacts with bpy and CO to give $Pt_4(\mu\text{-}PPh_2)_4(C_6F_5)_4$(bpy) and $[Pt_2(\mu\text{-}PPh_2)_2(C_6F_5)_2(CO)_2]_2$, respectively. The X-ray structures of $Pt_4(\mu\text{-}PPh_2)_3[\mu_3\text{-}PPh(1,2\text{-}\eta^2\text{-}Ph)\text{-}\kappa^3P](C_6F_5)_4$ (Fig. 11) and the bpy derivative accompany this report [145].

The cluster $[Ni_{15}(\mu_{12}\text{-}Sb)(CO)_{24}]^{2-}$ has been prepared from the reaction of $[Ni_{16}(CO)_{16}]^{2-}$ with $SbCl_3$. The molecular structure of this Ni_{15} cluster consists of a distorted Sb-centered $Ni_{12}(\mu_{12}$-Sb) icosahedral moiety, which is capped by three Ni atoms on three adjacent triangular faces. Cyclic voltammetric measurements confirm the existence of multiple reduction waves that are ascribed to the tri-, tetra-, and penta-anions. The product dianion is unstable under CO, decomposing to a mixture of $Ni(CO)_4$ and a cluster tentatively formulated as $[Ni_6Sb(CO)_x]^{2-}$. The chemical reactivity and the redox properties of $[Ni_{15}(\mu_{12}\text{-}Sb)(CO)_{24}]^{2-}$ are compared to and contrasted with other Ni-centered icosahedral clusters [146]. The high-yield synthesis of $[Pd_{13}Ni_{10}(Ni_{3-x}Pd_x)(CO)_{34}]^{4-}$ from $[Ni_6(CO)_{12}]^{2-}$ with either $Pd(OAc)_2$ in DMF or $[Pd(MeCN)_4][BF_4]_2$ in DMSO has been reported. The low-temperature CCD X-ray structure of this cluster has been solved, and a qualitative structure/bonding analysis on this cluster has been carried out in order to correlate the cluster's geometry with the electron count [147]. The oxidation of $[Ni_{15}Sb(CO)_{24}]^{2-}$ in acetone solution containing $SbCl_3$ furnishes the high-nuclearity cluster $[Ni_{31}Sb_4(CO)_{40}]^{6-}$. X-ray diffraction analysis reveals that the cluster polyhedron possesses two interstitial Ni and four semi-interstitial Sb atoms with unprecedented stereochemistries [148]. The synthesis of the homoleptic carbonyl clusters $[Ni_{16}Pd_{16}(CO)_{40}]^{4-}$ and $[Ni_{26}Pd_{20}(CO)_{54}]^{6-}$ from $[Ni_6(CO)_{12}]^{2-}$ and Pd(II) complexes is described. Included in this report is the X-ray structure of the former cluster. Data from extended Hückel MO calculations and cluster reactivity results are presented [149]. The synthesis and structural characterization of the nanosized cluster $Pd_{145}(CO)_x(PEt_3)_{30}$ have been published. This cluster, which was isolated from the reduction of $Pd(PEt_3)_2Cl_2$, contains a capped three-shell 145-atom metal-core geometry of pseudo icosahedral symmetry [150].

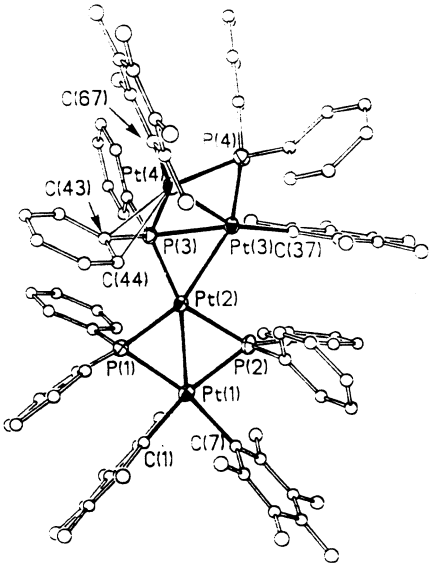

Fig. 11. X-ray structure of $Pt_4(\mu\text{-}PPh_2)_3[\mu_3\text{-}PPh(1,2\text{-}\eta^2\text{-}Ph)\text{-}\kappa^3P](C_6F_5)_4$. Reprinted with permission from Organometallics. Copyright 2000 American Chemical Society.

3. Heterometallic clusters

3.1. Trinuclear clusters

The self-assembly reactions of the ether chain-bridged salts $[\{W(CO)_3\}_2\{\eta^5\text{-}C_5H_4CH_2(CH_2OCH_2)_nCH_2C_5H_4\text{-}\eta^5\}]^{2-}$ with the chain-bridged double clusters $[WCoFe(\mu_3\text{-}S)(CO)_8]_2[\eta^5\text{-}C_5H_4CH_2(CH_2OCH_2)_nCH_2\text{-}C_5H_4\text{-}\eta^5]$ afford the new crown ether clusters $[W_2Fe(\mu_3\text{-}S)(CO)_7][\eta^5\text{-}C_5H_4CH_2(CH_2OCH_2)_nCH_2C_5H_4\text{-}\eta^5]$. The products have been characterized by elemental analysis, FAB mass spectrometry, and IR and NMR spectroscopies. The corresponding Mo derivatives have been synthesized, and the X-ray structures of two clusters have been determined [151]. A report describing the synthesis and redox behavior of the cluster crown ether complexes $[Mo_2Fe(\mu_3\text{-}S)(CO)_7]_n[\eta^5\text{-}C_5H_4CH_2(CH_2\text{-}OCH_2)_nCH_2C_5H_4\text{-}\eta^5]_n$ has appeared. Reaction pathways involved in the self-assembly sequence and the X-ray structure of $[Mo_2Fe(\mu_3\text{-}S)(CO)_7][\eta^5\text{-}C_5H_4CH_2\text{-}(CH_2OCH_2)_3CH_2C_5H_4\text{-}\eta^5]$ (Fig. 12) are presented and discussed [152].

Treatment of $[MeCpCr(\mu\text{-}SPh)_2]_2(\mu\text{-}Se)$ with $Co_2(CO)_8$ yields the mixed-metal heterochalcogenide cluster $(MeCpCr)_2(\mu\text{-}SPh)(\mu_3\text{-}S)(\mu_3\text{-}Se)Co(CO)_2$, whose X-ray structure confirms the triangular array of the

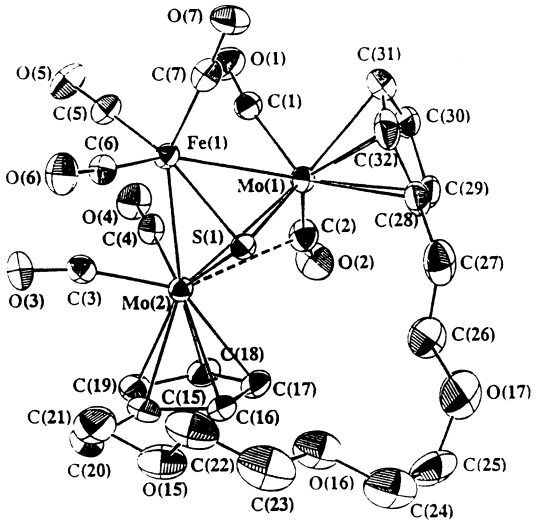

Fig. 12. X-ray structure of $[Mo_2Fe(\mu_3\text{-}S)(CO)_7][\eta^5\text{-}C_5H_4CH_2(CH_2OCH_2)_3CH_2C_5H_4\text{-}\eta^5]$. Reprinted with permission from Organometallics. Copyright 2000 American Chemical Society.

metal atoms and the capping μ_3-S and μ_3-Se moieties. The antiferromagnetic behavior of this cluster has been demonstrated over the temperature range of 290–80 K, and these studies have allowed for the determination of the exchange parameter ($-2J = 688$ cm^{-1}) [153]. The Mo_2Co complex $[\eta^5\text{-}C_5H_4C(O)PPh_2]Mo(CO)_3(\mu\text{-}PPh_2)Co(CO)_2Mo(CO)_2Cp$ has been isolated from the reaction between $(\eta^5\text{-}C_5H_4Li)(CO)_3MoCo(CO)_4$ and Ph_2PCl. The unusual bridging arrangements within the solid-state structure of this cluster are discussed [154].

The carbyne-bridged dimer $MnFe(\mu\text{-}CPh)(CO)_4(NO)Cp$ reacts with excess $Fe_2(CO)_9$ to produce $MnFe_2(\mu_3\text{-}CPh)(CO)_7(NO)Cp$. The related clusters $MnFeCo(\mu_3\text{-}CPh)(CO)_8Cp$ and $ReFeCo(\mu_3\text{-}CPh)(CO)_8Cp$ have been synthesized from $MnCo[C(CO)Ph](CO)_4(PPh_3)Cp$ and $ReFe[C(CO)Ph](CO)_3Cp_2$, respectively. The identities of these three clusters were ascertained by solution spectroscopic methods [155]. New $RePt_2$ and Re_2Pt_2 clusters have been isolated from the reaction between $Pt_2(\mu\text{-}S)_2(PPh_3)_4$ and $Re_2(CO)_{10}$ in the presence of Me_3NO and MeOH. The clusters $[Pt_2Re(\mu_3\text{-}S)_2(PPh_3)_4(CO)_3]^+[Re_3(\mu_3\text{-}OMe)(\mu\text{-}OMe)_3(CO)_9]^-$ and $Pt_2Re(\mu\text{-}OMe)_2(\mu_3\text{-}S)_2(PPh_3)_4(CO)_6$ are formed as the major products. The X-ray structure of the former Pt_2Re cluster reveals the presence of a Pt_2ReS_2 trigonal bipyramidal core with weak Re–Pt interactions. The reaction between $Pt_2(\mu\text{-}S)_2(PPh_3)_4$ and $MI_2(CO)_3(MeCN)_2$ (where M = Mo, W) affords the cluster salts $[Pt_2M(\mu_3\text{-}S)_2I(PPh_3)_4(CO)_4][MI_3(CO)_3]$, as a result of iodide migration. Two X-ray structures have been solved and their properties discussed [156]. The synthesis of the hydrido-bridged clusters $[(PMe_2Ph)_3(CO)HRe(\mu\text{-}H)_2M(\mu\text{-}H)_2ReH(CO)(PMe_2Ph)_3]^+$ (where M = Cu, Ag) from $ReH_3(CO)(PMe_2Ph)_3$ has been described [157].

Treatment of the phosphido-bridged complex $[Fe_2(CO)_6(PPh)_2]^{2-}$ with $PtCl_2$(dppe) gives the trimetallic *arachno* cluster $Fe_2(CO)_6(\mu_3\text{-}PPh)_2Pt$(dppe). The new Fe_2Pt cluster was characterized by IR and ^{31}P NMR spectroscopies, in addition to X-ray crystallography [158]. The homologous series of clusters $MPt_2(CO)_5(PPh_3)_2(PhC_2Ph)$ (where M = Fe, Ru, Os) have been prepared from $Pt(PPh_3)_2(PhC_2Ph)$ and $Fe(CO)_5$, $Ru_3(CO)_{12}$, and $Os_3(CO)_{12}$, respectively. All three products were characterized in solution by IR and NMR spectroscopies, and X-ray diffraction analyses. The cluster $Ru_2Pt(CO)_7(PPh_3)_2(PhC_2Ph)$ has also been isolated from the $Ru_3(CO)_{12}$ reaction. When this latter cluster is treated with H_2 in refluxing hexane, the tetranuclear cluster $H_2Ru_2Pt_2(CO)_8(PPh_3)_2$ is observed as the major isolable product. The catalytic activity of these clusters in the hydrosilation of diphenylacetylene to (*E*)-[(1,2-diphenyl)ethenyl]triethylsilane is reported. The experimental data suggest that the observed catalytic activity is principally derived from mononuclear platinum species as a result of cluster fragmentation [159].

The unsymmetrical trinuclear double bis(μ-alkynide) M–Pt–Pt (where M = Rh, Ir) complexes $(PEt_3)Cp^*M(\mu\text{-}1\kappa C^\alpha\text{:}\eta^2\text{-}C{\equiv}CR)_2Pt(\mu\text{-}2\kappa C^\alpha\text{:}\eta^2\text{-}C{\equiv}CR)_2Pt(C_6F_5)_2$ have been prepared from $(PEt_3)Cp^*M(\mu\text{-}1\kappa C^\alpha\text{:}\eta^2\text{-}C{\equiv}CR)_2Pt(C{\equiv}CR)_2$ and *cis*-$Pt(C_6F_5)_2(THF)_2$. The X-ray data from the $RhPt_2$ compound (where R = $SiMe_3$) reveal that the rhodium fragment, 'Cp*Rh(C≡CSi-$CSiMe_3)_2(PEt_3)$', acts as a chelating bidentate ligand towards the alkyne-bridged Pt_2 fragment [160].

3.2. Tetranuclear clusters

The synthesis of the heterometallic cubane clusters $Ti_3Cp^*_3(\mu_3\text{-}CR)(\mu_3\text{-}O)_3Mo(CO)_3$ (where R = H, Me) and $Ti_3Cp^*_3(\mu_3\text{-}NH)_3Mo(CO)_3$ has been described. DFT calculations have been performed on these clusters in order to study the bonding interactions inherent in the cubane core [161]. The early–late compounds $(acac)_3MOCCo_3(CO)_9$ (where M = Zr, Hf) have been prepared from $NaCo(CO)_4$ and $(acac)_3MCl$. These clusters are thermally robust and have been characterized in solution by IR and NMR (^1H and ^{13}C) spectroscopies. The X-ray structure of the zirconium analogue verifies the presence of a tetrahedrane core consisting of cobalt and alkylidyne groups [162].

High- and low-valent metal centers have been linked together in the new cluster compounds $Ru_3(CO)_{12}[Mo(NAr)_2]$ (where Ar = $C_6H_3X_2$-2,6; X = Me, ^{i}Pr, Cl). Treatment of the anionic cluster $[Ru_3(CO)_{11}]^{2-}$ with the bis(imido) complexes $Mo(NR)_2Cl_2(DME)$ affords the new 62-electron butterfly clusters. The X-ray structure of $Ru_3(CO)_{12}[Mo(NC_6H_3Me_2\text{-}2,6)_2]$ has

been determined and is discussed relative to other imido derivatives [163]. A review dealing with hydrocarbyl ligand transformations at WOs_3 clusters has appeared. The topics discussed include synthesis, reactivity, and solution dynamics of the ancillary ligands [164]. The synthesis and reactivity studies of the clusters $Co_2Mo_2(\mu_4\text{-CHCH})(\mu\text{-CO})_4(CO)_4[\eta^5\text{-}C_5H_4C(O)R]_2$ (where R = various groups) have been published. The nature of the cyclopentadienyl R group is shown to influence the reactivity of these clusters. The X-ray structure of $Co_2Mo_2(\mu_4\text{-CHCH})(CO)_8[\eta^5\text{-}C_5H_4C(O)\text{-}Me]_2$ has been solved, and the structural details of this butterfly cluster are fully described [165]. Decarbonylation of $HRu_3WCp(CO)_{11}BH$ using Me_3NO in the presence of PPh_3 leads to the phosphine-substituted clusters $HRu_3WCp(CO)_{11-x}(PPh_3)_xBH$ (where $x = 1$, 2). Treatment of $HRu_3(CO)_8(PPh_3)B_2H_5$ with $[CpW(CO)_3]_2$ also furnishes $HRu_3WCp(CO)_{10}\text{-}(PPh_3)BH$, whose X-ray structure was solved and shown to consist of a Ru_3W butterfly framework. The boron atom occupies a semi-interstitial position within the polyhedral core. The hydrogen distributions in these and related isoelectronic heterometallic clusters are correlated with the ^{1}H-NMR data [166]. The synthesis of the cluster compounds $[Cp(OC)_3W]C{\equiv}CC_2[Fe_2M(CO)_8\text{-}(PPh_3)]$ (where M = Rh, Ir) has been published [167]. The reaction between $Ru_3(CO)_{10}(MeCN)_2$ and $CpW(CO)_3(C{\equiv}CC{\equiv}CH)$ affords $Ru_3[\mu_3\text{-}HC_2C{\equiv}C\text{-}\{W(CO)_3Cp\}](\mu\text{-CO})(CO)_9$ as the initial product. This cluster readily transforms into $Ru_3(\mu\text{-H})[\mu_3\text{-}C_2C{\equiv}C\{W(CO)_3Cp\}](CO)_9$. Similar chemistry is observed with the dppm-substituted starting material $Ru_3(CO)_{10}$(dppm), and the three interconverting isomers of $Ru_3(\mu\text{-H})[\mu_3\text{-}C_2C{\equiv}C\{W(CO)_3Cp\}](\mu\text{-dppm})\text{-}(CO)_7$ have been studied in solution by NMR spectroscopy. The reactivity of $Ru_3(\mu\text{-H})[\mu_3\text{-}C_2C{\equiv}C\text{-}\{W(CO)_3Cp\}](CO)_9$ with $Fe_2(CO)_9$, $Co_2(CO)_8$, and $Ru_3(CO)_{12}$ has been investigated, and the new cluster products isolated and fully characterized in solution. Three X-ray structures accompany this report [168].

A new metal-chain assembly reaction has allowed for the formation of $(X)[Os(CO)_3(CN^tBu)]_3Mn(CO)_5$ (where X = Cl, Br, I) from the successive addition of $Os(CO)_4(CN^tBu)$ to $Mn(CO)_5X$. The X-ray structure of the iodo compound reveals the presence of a nearly linear chain of Os–Os–Os–Mn atoms. The results of ^{13}C-NMR studies of ^{13}CO enriched derivatives are presented and the chemical shifts discussed relative to the chain structure. A scheme depicting how the halide migrates from the manganese center to the osmium center accompanies this report [169]. The trirhenium cluster $[Re_3(\mu\text{-H})_3(\mu_3\text{-ampy})(CO)_9]^-$ reacts with the gold fragment $[Au(PPh_3)]^+$ to give $Re_3[\mu\text{-}Au(PPh_3)](\mu\text{-}H)_3(\mu_3\text{-ampy})(CO)_9$ and $Re_3[\mu\text{-}Au(PPh_3)](\mu_3\text{-H})(\mu\text{-}H)_2(\mu_3\text{-ampy})(CO)_9$. In the former product, each hydride ligand spans an edge of the Re_3 triangle, which is capped by the gold fragment. X-ray diffraction analysis of the latter cluster confirms that the gold atom spans a Re_2 edge, with two hydride ligands bridging the two other symmetry-related Re_2 edges. The remaining hydride ligand is shown to cap the Re_2Au triangle. This hydride interaction with the Re_2Au triangular face represents the first such example of a hydride ligand that is bonded to a gold center in this genre of cluster [170]. The protonation chemistry and ligand substitution reactivity of the butterfly oxo and sulfido clusters have been investigated. Treatment of $[Fe_3Mn(CO)_{12}(\mu_4\text{-O})]^-$ with PR_3 (where R = OMe, Me) and dppm gives $[Fe_3Mn(CO)_{10}(PR_3)_2(\mu_4\text{-O})]^-$ and $[Fe_3Mn(CO)_{10}\text{-}(dppm)(\mu_4\text{-O})]^-$, respectively. Whereas the latter cluster is protonated by HSO_3CF_3 at the Fe–Fe bond of the butterfly, the former two clusters do not show any protonation activity. The sulfido cluster $[Fe_3Mn(CO)_{12}(\mu_4\text{-S})]^-$ loses CO and Mn upon protonation to furnish the known cluster $H_2Fe_3(CO)_9(\mu_3\text{-S})$. The X-ray structure of $HFe_3Mn(CO)_{10}(dppm)(\mu_4\text{-O})$ was solved and the structural data have been compared with the parent cluster. All new clusters have been characterized in solution by IR and VT NMR (^{13}C and ^{31}P) spectroscopies [171]. The metalloborane complex $(Cp^*ReH_2)_2B_4H_4$, which is ultimately isolated from the reaction between Cp^*ReCl_4, $[Cp^*ReCl_3]_2$, or $[Cp^*ReCl_2]_2$ with $LiBH_4$, reacts with $Co_2(CO)_8$ to furnish the 6-sep hypoelectronic cluster $(Cp^*Re)_2Co_2(CO)_5B_4H_4$. The X-ray structure of this $Re_2Co_2B_4$ cluster (Fig. 13), which contains a sub*closo* electron count, is best described as a 24-valence-electron triple-decker complex and not the expected closed eight-vertex dodecahedron polyhedron. A mechanistic scheme that accounts for the formation of $(Cp^*Re)_2Co_2\text{-}(CO)_5B_4H_4$ is presented and discussed [172].

Metallic nanoparticles of Ru and Co have been obtained from the thermolysis of mesoporous xerogel or MCM-41 impregnated with $[Co_3Ru(CO)_{12}][NEt_4]$.

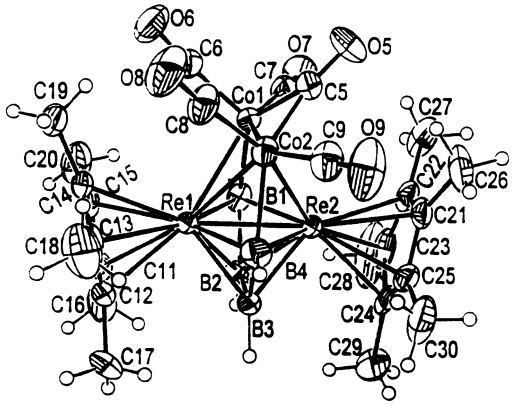

Fig. 13. X-ray structure of $(Cp^*Re)_2Co_2(CO)_5B_4H_4$. Reprinted with permission from Organometallics. Copyright 2000 American Chemical Society.

The magnetic properties of these nanoparticles were found to be superior to the analogous nanoparticles prepared via conventional ruthenium and cobalt salt precursors [173]. $Ru_3(CO)_{12}$ has been allowed to react with $Ir(^tBu_2PH)_3Cl$ in refluxing toluene to afford $Ru_3Ir(CO)_8(\mu_3\text{-}H)(\mu\text{-}Cl)_2(\mu\text{-}P^tBu_2)_2(^tBu_2PH)$, while the analogous reaction using $Au(^tBu_2PH)Cl$ in refluxing THF gives the cluster $Ru_3Au(CO)_{10}(\mu\text{-}Cl)(^tBu_2PH)$ in good yield. Both products contain a Ru_3M butterfly skeleton, as revealed by X-ray crystallography. With respect to the commonly found 62-electron count for butterfly polyhedra, the Ru_3Ir cluster contains 64-electrons and is electron rich, while the Ru_3Au product is electron poor given its 60-valence-electron count [174]. The reductive addition of $Pt(\eta^2\text{-}P\text{–}P)(\eta^2\text{-dba})$ (where P–P = dppf, dppr) to $Ru_3(CO)_9(\mu_3\text{-}S)_2$ yields the square clusters $PtRu_3(CO)_6(\mu\text{-}CO)_2(\eta^2\text{-}P\text{–}P)(\mu_4\text{-}S)_2$. Both products are rare examples of almost regularly octahedral heterometallic square clusters with two μ_4-S ligands that cap the faces of the $PtRu_3$ plane. The solid-state structure of each $PtRu_3$ cluster was ascertained by X-ray analysis [175]. The highly condensed cluster $(Cp^*Ru)_3Co(CO)_2(\mu_3\text{-}CO)B_3H_3$ has been obtained from the reaction of $(Cp^*Ru)_2(\mu\text{-}H)_2B_3H_6$ with $Co_2(CO)_8$. This 60-electron cluster is discussed relative to other tetranuclear metal clusters having different electron counts [176]. The luminescent cluster complex $[(C_6F_5)_6(\mu\text{-}OH)_3Pt_3HgCl]^{2-}$ has been synthesized from $Hg(NO_3)_2$ and $[Pt(C_6F_5)_3Cl]^{2-}$. X-ray diffraction analysis reveals the presence of a puckered central six-membered $Pt_3(\mu\text{-}OH)_3$ ring that is capped by the HgCl fragment, giving rise to three donor–acceptor Pt → Hg bonds. The UV–vis spectrum of the solid cluster is strongly luminescent, and the optical properties are attributed to emission involving a metal–metal (Pt–Hg) Hg) based charge transfer [177].

3.3. Pentanuclear clusters

The synthesis and X-ray structure of $Co_4MoCp(\mu_3\text{-}S^tBu)(\mu_3\text{-}S)(\mu_3\text{-}CO)(\mu\text{-}CO)_2(CO)_6$ have been published. This pentanuclear cluster was isolated in low yield as the only stable product from the reaction of $CoMoCp(CO)_7$ with $^tBuSS^tBu$. The cluster polyhedron exhibits an irregular tetrahedron of cobalt and molybdenum atoms [178]. A report on the coupling of coordinated acetylide ligands with and without CO using chalcogen-capped clusters has appeared. Thermolysis of $Fe_3(CO)_9(\mu_3\text{-}E)_2$ (where E = S, Se) with $CpMo(CO)_3(C{\equiv}CPh)$ (where M = Mo, W; Cp = Cp, Cp*) leads to the clusters $M_2Fe_3Cp_2(CO)_6(\mu_3\text{-}E)_2[\mu\text{-}CC(Ph)C(Ph)C]$ and $M_2Fe_2Cp_2(CO)_4(\mu_3\text{-}E)_2[\mu\text{-}CC(Ph)(CO)C(Ph)C]$. All of the products have been fully characterized in solution by IR and NMR spectroscopies, and the solid-state structures of two clusters have been determined. The X-ray structure and solution spectroscopic data on $W_2Fe_2Cp_2(CO)_4(\mu_3\text{-}S)_2[\mu\text{-}CC(Ph)(CO)C(Ph)C]$ confirm the presence of the 2,4-diphenyl-3-pentanone ligand that results from CO insertion into the coupled acetylide moieties [179]. Thermolysis of $Fe_2W(CO)_{10}(\mu_3\text{-}S)_2$ with $CpMo(CO)_3(CCPh)$ at 70 °C in the presence of oxygen affords $Cp_2Mo_2WFe_2(O)_2(S)_2(CO)_9(CCPh)_2$. The X-ray structure of this cluster (Fig. 14) shows that it consists of a triangular Fe_2W moiety, whose two faces are capped by the sulfido ligands. The redox properties of this Mo_2WFe_2 cluster were investigated by cyclic voltammetry and differential pulse voltammetry. The electron-transfer processes are discussed relative to specific metal sites [180].

A report on the use of carbonylcyanometalates as building blocks for heterometallic clusters has appeared. The structure of $Ru_3(\mu_3\text{-}NC)MnCp(CO)_2(\mu\text{-}AuPPh_3)(CO)_{10}$ was solved and shown to consist of a Ru_3Au butterfly core where the Ru–Ru hinge is bridged by the N-bonded $NCMnCp(CO)_2$ moiety. Thermolysis of the octanuclear cluster $[(OC)Pd(\mu\text{-}NC)MnCp(CO)_2]_4$ was found to take place by fragmentation, yielding bimetallic particles. EDAX and ESCA data confirm that the particles are homogeneous in nature and mostly metallic palladium and manganese in the form of manganese oxides [181].

3.4. Hexanuclear clusters

The synthesis and structure of the molybdenum–cobalt cluster $[Mo_3Co_3(\mu_6\text{-}C)(\mu\text{-}CO)_3(CO)_{15}]^{2-}$ have been described. This carbide cluster has been isolated in 3% yield from the reaction of $ClCCo_3(CO)_9$ with $Mo(CO)_3(MeCN)_3$. The octahedral core contains three

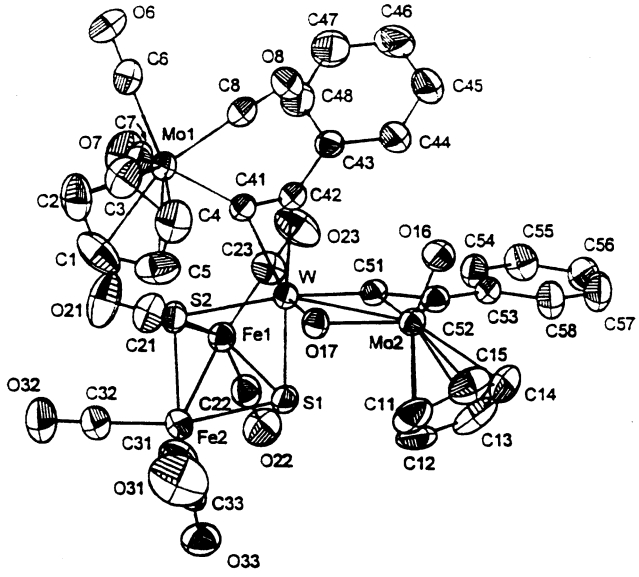

Fig. 14. X-ray structure of $Cp_2Mo_2WFe_2(O)_2(S)_2(CO)_9(CCPh)_2$. Reprinted with permission from Organometallics. Copyright 2000 American Chemical Society.

Mo and three Co centers arranged in facial positions [182]. Treatment of $[RhCl(CO)_2]_2$ with $[Fe_3(CO)_9C_2Fe(CO)_4]^{2-}$ yields the new monocarbide cluster $[Fe_3Rh_3(CO)_{15}C]^-$, whose identity was ascertained by IR spectroscopy and FAB-MS data [183]. The reaction of 1,8-bis(phenylethynyl)naphthalene with $Pt_2Ru_4(CO)_{18}$ leads to cluster fragmentation and production of $Ru_2(CO)_6(\mu\text{-}\eta^2\text{-}C_{10}H_6C_4Ph_2)$ and $Ru_2Pt(CO)_6(\mu\text{-}\eta^2\text{-}C_{10}H_6C_4Ph_2)_2$. The molecular structure of each product has been determined by X-ray crystallography. The latter product contains a non-linear array of Ru–Pt–Ru atoms that are held together by donor–acceptor Ru→Pt bonds [184]. CO substitution in $PtRu_5(CO)_{16}(\mu_6\text{-C})$ by PMe_2Ph leads to $PtRu_5(CO)_{16-n}(PMe_2Ph)_n(\mu_6\text{-C})$ (where $n = 1, 2$). These products have been isolated and characterized in solution by IR and NMR spectroscopies, in addition to X-ray crystallography. VT NMR analysis of $PtRu_5(CO)_{15}(PMe_2Ph)(\mu_6\text{-C})$ reveals that a facile intramolecular exchange exists that scrambles the phosphine ligand between the platinum and ruthenium centers at elevated temperatures. A scheme outlining the exchange process is proposed and fully discussed [185]. A series of clusters having the formula $[Fe_2(\mu\text{-CO})(CO)_6(\mu\text{-}PPh_2)Cu]_2(P–P)$ (where P–P = dppm, dppip, dppe, dppp, dppb) have been prepared from $[Fe_2(CO)_6(\mu\text{-CO})(\mu\text{-}PPh_2)]^-$ and $[Cu(MeCN)_4]^+$, followed by treatment with the desired diphosphine ligand. All of these new compounds have been characterized by IR and ^{31}P-NMR spectroscopies and cyclic voltammetry. The X-ray structure of the dppp derivative has been solved and its molecular structure discussed [186]. The polynuclear adduct $[Pt_2Ag_4(C{\equiv}C^tBu)_8(bpy)]_\infty$ has been obtained from the reaction of $Pt_2Ag_4(C{\equiv}C^tBu)_8$ and bpy. The X-ray structure of the polymer product consists of long-range, secondary misdirected Ag···N interactions between the cluster units and the bpy ligand. The polymer is highly emissive in the solid state and frozen solution. Details on the excitation and emission spectra are fully discussed [187].

3.5. Higher nuclearity clusters

The synthesis of $[Co_6C(CO)_{15}(AuPPh_3)]^-$ from $[Co_6(CO)_{12}]^{2-}$ and $AuCl(PPh_3)$ is reported. The cluster polyhedron is based on a Co_6C trigonal prism, which processes a capping $AuPPh_3$ moiety. A second $[AuPPh_3]^+$ fragment adds to this cluster to afford $Co_6C(CO)_{15}(AuPPh_3)_2$. The crystal structure of this cluster consists of a cobalt octahedron that has one face capped by an $Au_2(PPh_3)_2$ unit. The redox properties of both gold clusters have been investigated by cyclic voltammetry and coulometric analysis [188]. A paper describing the cluster build-up reactions of $[Os_7(CO)_{20}]^{2-}$ with digold reagents has appeared. The gold complexes $[Au_2(P–P)]^{2+}$ (where P–P = various bidentate phosphines) react with $[Os_7(CO)_{20}]^{2-}$ to yield the cluster compounds $Os_7(CO)_{20}[Au_2(P–P)]$, which on standing in solution lose CO to furnish $Os_7(CO)_{19}[Au_2(P–P)]$. The X-ray structure of the dppm derivative reveals that the metal core is based on an Os_7 edge-bridged bicapped tetrahedron with two μ_3-Au atoms capping adjacent triangular Os_3 faces. The reaction of the hydrido carbide cluster $[Os_7(H)C(CO)_{19}]^-$ with $[Au_2(dppm)]^{2+}$ in the presence of base to give the neutral cluster $Os_7C(CO)_{19}[Au_2(dppm)]$. The IR and NMR data ($^1H$ and ^{31}P) for seven new Os_7Au_2 clusters are discussed [189]. The synthesis, X-ray structure, and luminescent behavior of $[Ag\{Au(\mu\text{-}C^2,N^3\text{-bzim})_3\}_2][BF_4]$ are presented and discussed [190].

Treatment of $Os_6(CO)_{18}$ with Me_3NO in the presence of $[Au_2dppm][Cl]_2$ yields the new octanuclear cluster $Os_6(CO)_{17}(Au_2dppm)$. Sodium amalgam reduction of $Os_6(CO)_{17}(Au_2dppm)$, followed by treatment with $[CpRu(MeCN)_3][PF_6]$, gives the decanuclear clusters $Os_6(CO)_{17}(Au_2dppm)(CpRu)_2$ and $Os_6(CO)_{16}(Au_2dppm)(CpRu)_2$. The former $Os_6Au_2Ru_2$ cluster loses CO in refluxing toluene to produce the latter cluster. The molecular and crystal structures of $Os_6(CO)_{17}(Au_2dppm)$ and $Os_6(CO)_{17}(Au_2dppm)(CpRu)_2$ have been determined by single-crystal X-ray analyses [191]. The construction of nanoscale super clusters of clusters assembled around a dendritic core has been fully described. Through the use of the internal organic scaffold DAB-*dendr*-$\{N(CH_2PPh_2)_6\}_{16}$, the new complexes DAB-*dendr*-$\{N(CH_2PPh_2)_6\}_{16}[\mu_3\text{-}\eta^1,\eta^1,\eta^1\text{-}Ru_5C(CO)_{12}]_{16}$ and DAB-*dendr*-$\{N(CH_2PPh_2)_6\}_{16}[\mu_3\text{-}\eta^1,\eta^1,\eta^1\text{-}Au_2Ru_6C(CO)_{16}]_{16}$ have been prepared, and the HRTEM images of both derivatives have been recorded and the data discussed. The X-ray structures of the model clusters $[(CH_2)_4N(CH_2PPh_2)_2][Ru_5C(CO)_{15}]_2$ and $[PhCH_2N(CH_2PPh_2)_2][Au_2Ru_6C(CO)_{16}]$ have been determined, and their structures were employed in a discussion concerning the spectroscopic properties of the dendritic derivatives [192]. Chemical reduction of $Os_6(CO)_{17}(Au_2dppm)$, followed by treatment with $[Au_2dppm][NO_3]$, gives two isomers of $Os_6(CO)_{17}(Au_2dppm)_2$. Use of $[AuPPh_3][NO_3]$ affords two isomers of the related cluster $Os_6(CO)_{17}(Au_2dppm)(AuPPh_3)_2$. These new clusters have been fully characterized in solution by IR and NMR spectroscopies and FAB mass spectrometry. The solid-state structure of one of the isomers of $Os_6(CO)_{17}(Au_2dppm)_2$ has been solved. The six osmium atoms define an octahedron, in comparison to the bicapped tetrahedral geometry found in the parent cluster. The overall decametal core is best viewed as an octahedron fused with a capped square based pyramid [193]. The synthesis and X-ray structure of $Fe_5C(CO)_{14}[HgMoCp(CO)_3](AuPPh_3)$ are reported. This and related clusters have been prepared from

$[Fe_5C(CO)_{14}(HgM)]^-$ [where M = $CpMo(CO)_3$, $CpW(CO)_3$] and $[M'(PPh_3)]^+$ (where M′ = Cu, Ag, Au). Data from VT NMR and Mössbauer investigations are presented [194].

Treatment of $[Ni_6(CO)_{12}]^{2-}$ with $[Rh(COD)Cl]_2$ affords in sequence $[Ni_{10}Rh(CO)_{19}]^{3-}$ and $[Ni_9Rh_3(CO)_{22}]^{3-}$ with good selectivity. Degradation of $[Ni_9Rh_3(CO)_{22}]^{3-}$ under CO gives $[Ni_6Rh_3(CO)_{17}]^{3-}$, which may also be independently prepared from $[Rh(CO)_4]^-$ in the presence of excess $Ni(CO)_4$. All three trianions have been isolated and their crystal and molecular structures established by X-ray diffraction analyses [195]. A review discussing the reactivity of the segregated bimetallic cluster $Pt_3Ru_6(CO)_{20}(\mu_3\text{-}PhC_2Ph)(\mu\text{-}H)_2$ in alkyne hydrogenations and hydrosilations has appeared [196]. The boride cluster [HRu4(CO)12BH][PPN] reacts with $[Cu(MeCN)_4]^+$ to produce [PPN][{HRu4(CO)12B}2Cu4(μ-Cl)][Cl], whose X-ray structure accompanies this report. When the same reaction is carried out with $[Ag(MeCN)_4]^+$ or $AgBF_4$, the observed product is [{HRu4(CO)12BH}2Ag]−. The IR, NMR, and structural data for these two clusters are discussed [197]. The high-yield synthesis of $[Ir_7Ru_3(CO)_{23}]^-$ from $[Ir_6(CO)_{15}]^{2-}$ and $Ru_3(CO)_{12}$ in the presence of *p*-toluenesulfonic acid is reported. The X-ray structure reveals that this cluster possesses an octahedral core of iridium atoms that is face capped by the remaining iridium atom and the three ruthenium atoms. The role of the *p*-toluenesulfonic acid is to assist in the degradation of the Ir_6 dianion. $[Ir_7Ru_3(CO)_{23}]^-$ has been allowed to react with $AuCl(PPh_3)$ in the presence of $AgOSO_2CF_3$ to give $Ir_7Ru_3(CO)_{23}(AuPPh_3)$. The gold–phosphine ligand is shown to coordinate to the apical iridium atom of the parent monoanion [198]. The compound $[\{Cp^*Ir(CO)\}_6Hg_8]^{6+}$, which contains an Ir_6Hg_6 twelve-membered ring, has been prepared from $Cp^*Ir(CO)_2$ and $Hg(O_2CCF_3)_2$ in CH_2Cl_2. A discussion on the molecular structure of this cluster is presented [199]. The high-nuclearity cluster $Pd_8Ru_{10}C_2(CO)_{27}(allyl)_4$ has been synthesized in good yield from $[Ru_5C(CO)_{14}]^{2-}$ and $[Pd(allyl)Cl]_2$. The analogous reaction between $[Ru_6C(CO)_{16}]^{2-}$ and $[Pd(MeCN)_4]^+$ furnishes $[Pd_2Ru_{12}C_2(CO)_{30}]^{2-}$ and $[Pd_4Ru_{12}C_2(CO)_{32}]^{2-}$ depending upon the reaction conditions. Chemical and electrochemical redox studies indicate that these reactions do not result from a simple combination reaction between the cationic and anionic reagents but rather from redox condensation processes. The X-ray structures of all three cluster products have been solved and their structural details fully discussed [200].

References

[1] M.M. Bower, Diss. Abstr. Sect. B 60 (2000) 5083(DA9948592).
[2] R.J. Hall, Diss. Abstr. Sect. B 60 (2000) 3943(DA9943320).
[3] D.H. Hamilton, Diss. Abstr. Sect. B 60 (2000) 5508-(DA9953036).
[4] C.C. Borg-Breen, Diss. Abstr. Sect. B 61 (2000) 2526-(DA9968549).
[5] L.S.E.B. Collins, Diss. Abstr. Sect. B 60 (2000) 3273(DA9938132).
[6] B.E. Collins, Diss. Abstr. Sect. B 60 (2000) 3273(DA9938131).
[7] B.K. Breedlove, Diss. Abstr. Sect. B 60 (2000) 5507-(DA9952062).
[8] M.T. Blankenbuehler, Diss. Abstr. Sect. B 60 (2000) 6094-(DA9957019).
[9] J.W. Raebiger, Diss. Abstr. Sect. B 60 (2000) 5512(DA9949790).
[10] B.D. Chandler, Diss. Abstr. Sect. B 60 (2000) 3941(DA9941714).
[11] G. Panjabi, Diss. Abstr. Sect. B 61 (2000) 1947(DA9969622).
[12] J.P. Sarasa, J.M. Poblet, M. Bénard, Organometallics 19 (2000) 2264.
[13] O.I. Guzyr, J. Prust, H.W. Roesky, C. Lehmann, M. Teichert, F. Cimpoesu, Organometallics 19 (2000) 1549.
[14] B.P. Johnson, M. Schiffer, M. Scheer, Organometallics 19 (2000) 3404.
[15] R.D. Adams, O.-S. Kwon, J.L. Perrin, J. Organomet. Chem. 596 (2000) 102.
[16] G. D'Alfonso, D. Roberto, R. Ugo, C.L. Bianchi, A. Sironi, Organometallics 19 (2000) 2564.
[17] U. Brand, J.R. Shapley, Inorg. Chem. 39 (2000) 32.
[18] F. Kakiuchi, M. Matsumoto, M. Sonoda, T. Fukuyama, N. Chatani, S. Murai, N. Furukawa, Y. Seki, Chem. Lett. (2000) 750.
[19] M. Tobisu, N. Chatani, T. Asaumi, K. Amako, Y. Ie, Y. Fukumoto, S. Murai, J. Am. Chem. Soc. 122 (2000) 12663.
[20] F. Ragaini, S. Cenini, J. Mol. Catal. A 161 (2000) 31.
[21] B. Bonelli, S. Brait, S. Deabate, E. Garrone, R. Giordano, E. Sappa, F. Verre, J. Clust. Sci. 11 (2000) 307.
[22] D.D. Ellis, A. Franken, P.A. Jelliss, F.G.A. Stone, P.-Y. Yu, Organometallics 19 (2000) 1993.
[23] S. Brait, G. Gervasio, D. Marabello, E. Sappa, J. Chem. Soc. Dalton Trans. (2000) 989.
[24] P. Schooler, B.F.G. Johnson, L. Scaccianoce, J. Dannheim, H. Hopf, J. Chem. Soc. Dalton Trans. (2000) 199.
[25] A. Inagaki, T. Takemori, M. Tanaka, H. Suzuki, Angew. Chem. Int. Ed. Engl. 39 (2000) 404.
[26] L. Pereira, W.K. Leong, S.Y. Wong, J. Organomet. Chem. 609 (2000) 104.
[27] S. Aime, W. Dastrù, R. Gobetto, A. Viale, Inorg. Chem. 39 (2000) 2422.
[28] S. Aime, W. Dastrù, R. Gobetto, A. Viale, J. Organomet. Chem. 593–594 (2000) 135.
[29] L.P. Clarke, J.E. Davies, P.R. Raithby, M.-A. Rennie, G.P. Shields, E. Sparr, J. Organomet. Chem. 609 (2000) 169.
[30] R.J. Hall, P. Serguievski, J.B. Keister, Organometallics 19 (2000) 4499.
[31] E. Lucenti, D. Roberto, C. Roveda, R. Ugo, A. Sironi, Organometallics 19 (2000) 1051.
[32] S. Aime, A. Arce, R. Gobetto, D. Giusti, M. Stchedroff, Chem. Commun. (2000) 1425.
[33] H. Nagashima, A. Suzuki, T. Iura, K. Ryu, K. Matsubara, Organometallics 19 (2000) 3579.
[34] M.I. Bruce, B.W. Skelton, A.H. White, N.N. Zaitseva, J. Chem. Soc. Dalton Trans. (2000) 881.
[35] S. Aime, A.J. Arce, D. Giusti, R. Gobetto, J.W. Steed, J. Chem. Soc. Dalton Trans. (2000) 2215.
[36] D.B. Brown, B.F.G. Johnson, C.M. Martin, A.E.H. Wheatley, J. Chem. Soc. Dalton Trans. (2000) 2055.
[37] J.P.H. Charmant, P. Crawford, P.J. King, R. Quesada-Pato, E. Sappa, J. Chem. Soc. Dalton Trans. (2000) 4390.

[38] J.P.H. Charmant, G. Davies, P.J. King, J.R. Wigginton, E. Sappa, Organometallics 19 (2000) 2330.
[39] M.J. Bakker, F.W. Vergeer, F. Hartl, O.S. Jina, X.-Z. Sun, M.W. George, Inorg. Chim. Acta 300–302 (2000) 597.
[40] R.D. Adams, B. Qu, Organometallics 19 (2000) 2411.
[41] M.A. Lynn, D.L. Lichtenberger, J. Clust. Sci. 11 (2000) 169.
[42] H.-F. Hsu, J.R. Shapley, Inorg. Chim. Acta 599 (2000) 97.
[43] H. Song, K. Lee, J.T. Park, H.Y. Chang, M.-G. Choi, J. Organomet. Chem. 599 (2000) 49.
[44] E. Hunstock, M.J. Calhorda, P. Hirva, T.A. Pakkanen, Organometallics 19 (2000) 4624.
[45] P.J. Dyson, J.E. McGrady, M. Reinhold, B.F.G. Johnson, J.S. McIndoe, P.R.R. Langridge-Smith, J. Clust. Sci. 11 (2000) 391.
[46] B.K. Das, M.G. Kanatzidis, Polyhedron 19 (2000) 1995.
[47] D.D. Ellis, A. Franken, T.D. McGrath, F.G.A. Stone, J. Organomet. Chem. 614–615 (2000) 208.
[48] W. Uhl, M. Benter, M. Prött, J. Chem. Soc. Dalton Trans. (2000) 643.
[49] R.D. Adams, B. Qu, Organometallics 19 (2000) 4090.
[50] Y.-K. Yan, W. Koh, C. Jiang, W.K. Leong, T.S.A. Hor, Polyhedron 19 (2000) 641.
[51] H. Brunner, J. Wachter, R. Wanninger, M. Zabel, J. Organomet. Chem. 603 (2000) 135.
[52] J. Zhang, W.K. Leong, J. Chem. Soc. Dalton Trans. (2000) 1249.
[53] U. Flörke, H. Egold, M. Schraa, Acta Crystallogr. C56 (2000) 760.
[54] R.W. Eveland, D.F. Shriver, Inorg. Chim. Acta 309 (2000) 10.
[55] K.M. Hanif, S.E. Kabir, M.A. Mottalib, M.B. Hursthouse, K.M.A. Malik, E. Rosenberg, Polyhedron 19 (2000) 1073.
[56] V.P. Kirin, V.A. Maksakov, A.V. Virovets, A.V. Golovin, Inorg. Chem. Commun. 3 (2000) 224.
[57] J. Akter, K.A. Azam, S.E. Kabir, K.M.A. Malik, M.A. Mottalib, Inorg. Chem. Commun. 3 (2000) 553.
[58] E.V. García-Báez, M.J. Rosales-Hoz, H. Nöth, I. Haiduc, C. Silvestru, Inorg. Chem. Commun. 3 (2000) 173.
[59] M. Shieh, H.-S. Chen, H.-H. Chi, C.-H. Ueng, Inorg. Chem. 39 (2000) 5561.
[60] S.F.A. Kettle, E. Diana, R. Rossetti, E. Boccaleri, U.A. Jayasooryia, P.L. Stanghellini, Inorg. Chem. 39 (2000) 5690.
[61] C.J. Adams, L.P. Clarke, A.M. Martín-Castro, P.R. Raithby, G.P. Shields, J. Chem. Soc. Dalton Trans. (2000) 4015.
[62] R.D. Adams, O.-S. Kwon, J.L. Perrin, Organometallics 19 (2000) 2246.
[63] K. Biradha, V.M. Hansen, W.K. Leong, R.K. Pomeroy, M.J. Zaworotko, J. Clust. Sci. 11 (2000) 285.
[64] R. Buntem, J.F. Gallagher, J. Lewis, P.R. Raithby, M.-A. Rennie, G.P. Shields, J. Chem. Soc. Dalton Trans. (2000) 4297.
[65] D.H. Hamilton, J.R. Shapley, Organometallics 19 (2000) 761.
[66] S.E. Kabir, K.M.A. Malik, E. Rosenberg, T.A. Siddiquee, Inorg. Chem. Commun. 3 (2000) 140.
[67] H. Adams, S.C.M. Agustinho, B.E. Mann, S. Smith, J. Organomet. Chem. 607 (2000) 175.
[68] H. Wadepohl, S. Gebert, H. Pritzkow, J. Organomet. Chem. 614–615 (2000) 158.
[69] E.W. Ainscough, A.M. Brodie, A.K. Burrell, S.M.F. Kennedy, J. Organomet. Chem. 609 (2000) 2.
[70] R. Hourihane, G. Gray, T. Spalding, T. Deeney, J. Organomet. Chem. 595 (2000) 191.
[71] D. Cauzzi, C. Graiff, C. Massera, G. Predieri, A. Tiripicchio, Inorg. Chim. Acta 300–302 (2000) 471.
[72] W.K. Leong, G. Chen, J. Chem. Soc. Dalton Trans. (2000) 4442.
[73] S.E. Kabir, K.M.A. Malik, E. Molla, M.A. Mottalib, J. Organomet. Chem. 616 (2000) 157.
[74] W.-Y. Yeh, C.-C. Yang, S.-M. Peng, G.-H. Lee, J. Chem. Soc. Dalton Trans. (2000) 1649.
[75] C. Allasia, M. Castiglioni, R. Giordano, E. Sappa, F. Verre, J. Clust. Sci. 11 (2000) 493.
[76] J.T. McFadden, W.G. Feighery, J. Clust. Sci. 11 (2000) 373.
[77] D.J. Darensbourg, F.A. Beckford, J.H. Reibenspies, J. Clust. Sci. 11 (2000) 95.
[78] H.G. Ang, S.G. Ang, X. Wang, J. Chem. Soc. Dalton Trans (2000) 3429.
[79] E. Alonso, D. Astruc, J. Am. Chem. Soc. 122 (2000) 3222.
[80] S. Aime, M. Férriz, R. Gobetto, E. Valls, Organometallics 19 (2000) 707.
[81] M.J. Bakker, F. Hartl, D.J. Stufkens, O.S. Jina, X.-Z. Sun, M.W. George, Organometallics 19 (2000) 4310.
[82] W.-Y. Wong, S.-H. Cheung, S.-M. Lee, S.-Y. Leung, J. Organomet. Chem. 596 (2000) 36.
[83] V.A. Maksakov, V.P. Kirin, P.A. Petukhov, T.V. Rybalova, Y.V. Gatilov, A.V. Tkachev, J. Organomet. Chem. 604 (2000) 1.
[84] G. Sánchez-Cabrera, E.V. García-Báez, M.J. Rosales-Hoz, J. Organomet. Chem. 599 (2000) 313.
[85] S.T. Beatty, B. Bergman, E. Rosenberg, W. Dastrú, R. Gobetto, L. Milone, A. Viale, J. Organomet. Chem. 593–594 (2000) 226.
[86] E. Rosenberg, M.J. Abedin, D. Rokhsana, D. Osella, L. Milone, C. Nervi, J. Fiedler, Inorg. Chim. Acta 300–302 (2000) 769.
[87] K.A. Azam, R. Dilshad, S.E. Kabir, M.A. Mottalib, M.B. Hursthouse, K.M.A. Malik, Polyhedron 19 (2000) 1081.
[88] S.M.T. Abedin, K.I. Hardcastle, S.E. Kabir, K.M.A. Malik, M.A. Mottalib, E. Rosenberg, M.J. Abedin, Organometallics 19 (2000) 623.
[89] J.A. Cabeza, I. del Río, F. Grepioni, V. Riera, Organometallics 19 (2000) 4643.
[90] M.-H. Chao, S. Kumaresan, Y.-S. Wen, S.-C. Lin, J.R. Hwu, K.-L. Lu, Organometallics 19 (2000) 714.
[91] H.-B. Zheng, S.-B. Miao, Z.-X. Wang, Z.-Y. Zhou, X.-G. Zhou, Polyhedron 19 (2000) 713.
[92] T. Gröer, M. Scheer, Organometallics 19 (2000) 3683.
[93] A. Bérces, O. Koentjoro, B.T. Sterenberg, J.H. Yamamoto, J. Tse, A.J. Carty, Organometallics 19 (2000) 4336.
[94] S. Kahlal, K.A. Udachin, L. Scoles, A.J. Carty, J.-Y. Saillard, Organometallics 19 (2000) 2251.
[95] P. Homanen, R. Persson, M. Haukka, T.A. Pakkanen, E. Nordlander, Organometallics 19 (2000) 5568.
[96] G. Süss-Fink, L. Plasseraund, A. Maisse-Francois, H. Stoeckli-Evans, H. Berke, T. Fox, R. Gautier, J.-Y. Saillard, J. Organomet. Chem. 609 (2000) 196.
[97] L.P. Clarke, J.E. Davies, P.R. Raithby, G.P. Shields, J. Chem. Soc. Dalton Trans. (2000) 4527.
[98] L.T. Byrne, J.P. Hos, G.A. Koutsantonis, B.W. Skelton, A.H. White, J. Organomet. Chem. 598 (2000) 28.
[99] W. Wang, P.J. Low, A.J. Carty, E. Sappa, G. Gervasio, C. Mealli, A. Ienco, E. Perez-Carreño, Inorg. Chem. 39 (2000) 998.
[100] S. Takemoto, S. Kuwata, Y. Nishibayashi, M. Hidai, Organometallics 19 (2000) 3249.
[101] K. Lee, C.H. Lee, H. Song, J.T. Park, H.Y. Chang, M.-G. Choi, Angew. Chem. Int. Ed. 39 (2000) 1801.
[102] M. Akita, M.-C. Chung, A. Sakurai, Y. Moro-oka, Chem. Commun. (2000) 1285.
[103] M.I. Bruce, M. Schulz, B.W. Skelton, A.H. White, J. Clust. Sci. 11 (2000) 79.
[104] P. Mathur, P. Payra, S. Ghose, M.M. Hossain, C.V.V. Satyanarayana, F.O. Chicote, R.K. Chadha, J. Organomet. Chem. 606 (2000) 176.
[105] M.I. Bruce, B.D. Kelly, B.W. Skelton, A.H. White, J. Organomet. Chem. 604 (2000) 150.
[106] J.H. Yamamoto, L. Scoles, K.A. Udachin, G.D. Enright, A.J. Carty, J. Organomet. Chem. 600 (2000) 84.
[107] D.H. Farrar, A.J. Poë, Y. Zheng, Inorg. Chim. Acta 300–302 (2000) 668.
[108] R.D. Adams, B. Captain, W. Fu, Organometallics 19 (2000) 3670.

[109] P.J. Dyson, B.F.G. Johnson, J.S. McIndoe, P.R.R. Langridge-Smith, Inorg. Chem. 39 (2000) 2430.
[110] J.-H. Chung, G. Jordan, E.A. Meyers, S.G. Shore, Inorg. Chem. 39 (2000) 568.
[111] B.F.G. Johnson, K.M. Sanderson, D.S. Shephard, D. Ozkaya, W. Zhou, H. Ahmed, M.D.R. Thomas, L. Gladden, M. Mantle, Chem. Commun. (2000) 1317.
[112] B.F.G. Johnson, C.M.G. Judkins, J.M. Matters, D.S. Shephard, S. Parsons, Chem. Commun. (2000) 1549.
[113] S. Hermans, B.F.G. Johnson, Chem. Commun (2000) 1955.
[114] P.J. Dyson, N. Feeder, B.F.G. Johnson, J.S. McIndoe, P.R.R. Langridge-Smith, J. Chem. Soc. Dalton Trans. (2000) 1813.
[115] D.M. Norton, D.F. Shriver, Inorg. Chem. 39 (2000) 5118.
[116] S.L. Shea, T. Jelínek, B. Stíbr, M. Thornton-Pett, J.D. Kennedy, Inorg. Chem. Commun. 3 (2000) 169.
[117] V. Calvo-Perez, E. Spodine, Inorg. Chim. Acta 310 (2000) 133.
[118] D. Osella, C. Nervi, L. Milone, F. Galeotti, A. Vessiéres, G. Jaouen, J. Organomet. Chem. 593–594 (2000) 232.
[119] L. Markó, G. Gervasio, D. Marabello, G. Szalontai, J. Clust. Sci. 11 (2000) 29.
[120] S. Onaka, Y. Katsukawa, H. Muto, J. Coord. Chem. 51 (2000) 33.
[121] J. Zhang, Y.-H. Zhang, X.-N. Chen, E.-R. Ding, Y.-Q. Yin, Organometallics 19 (2000) 5032.
[122] H. Seino, Y. Mizobe, M. Hidai, Organometallics 19 (2000) 3631.
[123] N. Jeong, S.H. Hwang, Angew. Chem. Int. Ed. Engl. 39 (2000) 636.
[124] M.E. Krafft, L.V.R. Boñaga, Angew. Chem. Int. Ed. Engl. 39 (2000) 3676.
[125] A. Caiazzo, R. Settambolo, L. Pontorno, R. Lazzaroni, J. Organomet. Chem. 599 (2000) 298.
[126] O.S. Alexeev, D.-W. Kim, B.C. Gates, J. Mol. Catal. A 162 (2000) 67.
[127] B.C. Gates, J. Mol. Catal. A 163 (2000) 55.
[128] G. Liu, M. Garland, J. Organomet. Chem. 613 (2000) 124.
[129] J. Blum, F. Gelman, R. Abu-Reziq, I. Miloslavski, H. Schumann, D. Avnir, Polyhedron 19 (2000) 509.
[130] L.J. Farrugia, J. Clust. Sci. 11 (2000) 39.
[131] Q. Xu, S. Inoue, Y. Souma, H. Nakatani, J. Organomet. Chem. 606 (2000) 147.
[132] C. Sizun, P. Kempgens, J. Raya, K. Elbayed, P. Granger, J. Rosé, J. Organomet. Chem. 604 (2000) 27.
[133] S. Detti, T. Lumini, R. Roulet, K. Schenk, R. Ros, A. Tassan, J. Chem. Soc. Dalton Trans. (2000) 1645.
[134] P.B. Hitchcock, J.F. Nixon, M.D. Vargas, C.M. Ziglio, J. Chem. Soc. Dalton Trans. (2000) 2527.
[135] N. Nawar, J. Organomet. Chem. 602 (2000) 137.
[136] R.D. Pergola, L. Garlaschelli, S. Martinengo, M. Manassero, M. Sansoni, J. Organomet. Chem. 593–594 (2000) 63.
[137] S.-W. Zhang, S. Takahashi, Chem. Commun. (2000) 315.
[138] F. Ragaini, A. Sironi, A. Fumagalli, Chem. Commun. (2000) 2117.
[139] A. Fumagalli, S. Martinengo, G. Bernasconi, L. Noriglia, V.G. Albano, M. Monari, C. Castellari, Organometallics 19 (2000) 5149.
[140] M. Beneke, L. Brabec, N. Jaeger, J. Nováková, G. Schulz-Ekloff, J. Mol. Catal. A 157 (2000) 151.
[141] R. Ros, A. Tassan, G. Laurenczy, R. Roulet, Inorg. Chim. Acta 303 (2000) 94.
[142] S. Pasynkiewicz, A. Pietrzykowski, B. Kryza-Niemiec, L. Jerzykiewicz, J. Organomet. Chem. 593–594 (2000) 245.
[143] A. Pietrzykowski, P. Buchalski, L.B. Jerzykiewicz, J. Organomet. Chem. 597 (2000) 133.
[144] S. Pasynkiewicz, A. Pietrzykowski, B. Kryza-Niemiec, R. Anulewicz-Ostrowska, J. Organomet. Chem. 613 (2000) 37.
[145] E. Alonso, J. Forniés, C. Fortuño, A. Martín, A.G. Orpen, Organometallics 19 (2000) 2690.
[146] V.G. Albano, F. Demartin, C. Femoni, M.C. Iapalucci, G. Longoni, M. Monari, P. Zanello, J. Organomet. Chem. 593–594 (2000) 325.
[147] N.T. Tran, M. Kawano, D.R. Powell, L.F. Dahl, J. Chem. Soc. Dalton Trans. (2000) 4138.
[148] C. Femoni, M.C. Iapalucci, G. Longoni, P.H. Svensson, Chem. Commun. (2000) 655.
[149] C. Femoni, M.C. Iapalucci, G. Longoni, P.H. Svensson, J. Wolowska, Angew. Chem. Int. Ed. Engl. 39 (2000) 1635.
[150] N.T. Tran, D.R. Powell, L.F. Dahl, Angew. Chem. Int. Ed. Engl. 39 (2000) 4121.
[151] L.-C. Song, D.-S. Guo, Q.-M. Hu, J. Sun, J. Organomet. Chem. 616 (2000) 140.
[152] L.-C. Song, D.-S. Guo, Q.-M. Hu, X.-Y. Huang, Organometallics 19 (2000) 960.
[153] A.A. Pasynskii, F.S. Denisov, Y.V. Torubaev, N.I. Semenova, V.M. Novotortsev, O.G. Ellert, S.E. Nefedov, K.A. Lyssenko, J. Organomet. Chem. 612 (2000) 9.
[154] R.S. Dickson, G.D. Fallon, W.R. Jackson, A. Polas, J. Organomet. Chem. 607 (2000) 156.
[155] Y. Tang, J. Sun, J. Chen, Organometallics 19 (2000) 72.
[156] H. Liu, C. Jiang, J.S.L. Yeo, K.F. Mok, L.K. Liu, T.S.A. Hor, Y.K. Yan, J. Organomet. Chem. 595 (2000) 276.
[157] S. Luo, C.J. Burns, G.J. Kubas, J.C. Bryan, R.H. Crabtree, J. Clust. Sci. 11 (2000) 189.
[158] W.H. Watson, A. Nagl, M.-J. Don, M.G. Richmond, J. Chem. Crystallogr. 30 (2000) 233.
[159] R.D. Adams, U. Bunz, B. Captain, W. Fu, W. Steffen, J. Organomet. Chem. 614–615 (2000) 75.
[160] J.R. Berenguer, E. Equizábal, L.R. Falvello, J. Forniés, E. Lalinde, A. Martín, Organometallics 19 (2000) 490.
[161] A. Abarca, M. Galakhov, P. Gómez-Sal, A. Martín, M. Mena, J.-M. Poblet, C. Santamaría, J.P. Sarasa, Angew. Chem. Int. Ed. Engl. 39 (2000) 534.
[162] K. Kluwe, K.-H. Thiele, A. Sorkau, A. Sisak, B. Neumüller, J. Organomet. Chem. 604 (2000) 68.
[163] S. Ali, A.J. Carty, A.J. Deeming, G.D. Enright, G. Hogarth, Chem. Commun. (2000) 123.
[164] J.T. Park, J.R. Shapley, K. Lee, H. Song, J. Clust. Sci. 11 (2000) 343.
[165] J. Zhang, X.-N. Chen, E.-R. Ding, Y.-Q. Yin, J. Coord. Chem. 51 (2000) 283.
[166] C.E. Housecroft, D.M. Nixon, A.L. Rheingold, J. Organomet. Chem. 609 (2000) 89.
[167] M.I. Bruce, B.G. Ellis, B.W. Skelton, A.H. White, J. Organomet. Chem. 607 (2000) 137.
[168] M.I. Bruce, P.J. Low, N.N. Zaitseva, S. Kahlal, J.-F. Halet, B.W. Skelton, A.H. White, J. Chem. Soc. Dalton Trans. (2000) 2939.
[169] F. Jiang, H.A. Jenkins, G.P.A. Yap, R.K. Pomeroy, Inorg. Chem. Commun. 3 (2000) 685.
[170] J.A. Cabeza, V. Riera, R. Trivedi, Organometallics 19 (2000) 2043.
[171] C.K. Schauer, E.J. Voss, M. Sabat, D.F. Shriver, Inorg. Chim. Acta 300–302 (2000) 7.
[172] S. Ghosh, X. Lei, M. Shang, T.P. Fehlner, Inorg. Chem. 39 (2000) 5373.
[173] F. Schweyer, P. Braunstein, C. Estournés, J. Guille, H. Kessler, J.-L. Paillaud, J. Rosé, Chem. Commun. (2000) 1271.
[174] H.-C. Böttcher, M. Graf, K. Merzweiler, C. Wagner, Polyhedron 19 (2000) 2593.
[175] S.-W.A. Fong, J.J. Vittal, T.S.A. Hor, Organometallics 19 (2000) 918.
[176] X. Lei, M. Shang, T.P. Fehlner, Organometallics 19 (2000) 4429.
[177] J.M. Casas, L.R. Falvello, J. Forniés, J. Gomez, A. Rueda, J. Organomet. Chem. 593–594 (2000) 421.

[178] J.D. King, M. Mays, M. McPartlin, S. Radojevic, V. Sarveswaran, G.A. Solan, Inorg. Chem. Commun 3 (2000) 159.
[179] P. Mathur, M.O. Ahmed, A.K. Dash, M.G. Walawalkar, V.G. Puranik, J. Chem. Soc. Dalton Trans. (2000) 2916.
[180] P. Mathur, S. Mukhopadhyay, M.O. Ahmed, G.K. Lahiri, S. Chakraborty, M.G. Walawalkar, Organometallics 19 (2000) 5787.
[181] P. Braunstein, B. Oswald, A. Tiripicchio, F. Ugozzoli, J. Chem. Soc. Dalton Trans. (2000) 2195.
[182] S. Kamiguchi, T. Chihara, J. Clust. Sci 11 (2000) 483.
[183] D.M. Norton, D.F. Shriver, J. Organomet. Chem. 614–615 (2000) 318.
[184] R.D. Adams, W. Fu, B. Qu, J. Clust. Sci. 11 (2000) 55.
[185] R.D. Adams, B. Captain, W. Fu, P.J. Pellechia, Chem. Commun. (2000) 937.
[186] M. Ferrer, O. Rossell, M. Seco, M. Soler, M. Font-Bardía, X. Solans, D. de Montauzon, J. Organomet. Chem. 598 (2000) 215.
[187] I. Ara, J. Forníes, J. Gómez, E. Lalinde, M.T. Moreno, Organometallics 19 (2000) 3137.
[188] R. Reina, O. Riba, O. Rossell, M. Seco, D. de Montauzon, M.A. Pellinghelli, A. Tiripicchio, M. Font-Bardía, X. Solans, J. Chem. Soc. Dalton Trans. (2000) 4464.
[189] Z. Ahkter, A.J. Edwards, S.L. Ingham, J. Lewis, A.M.M. Castro, P.R. Raithby, G.P. Shields, J. Clust. Sci. 11 (2000) 217.
[190] A. Burini, R. Bravi, J.P. Fackler, Jr., R. Galassi, T.A. Grant, M.A. Omary, B.R. Pietroni, R.J. Staples, Inorg. Chem. 39 (2000) 3158.
[191] Z. Akhter, A.J. Edwards, J.F. Gallagher, J. Lewis, P.R. Raithby, G.P. Shields, J. Organomet. Chem. 596 (2000) 204.
[192] N. Feeder, J. Geng, P.G. Goh, B.F.G. Johnson, C.M. Martin, D.S. Shephard, W. Zhou, Angew. Chem. Int. Ed. Engl. 39 (2000) 1661.
[193] Z. Akhter, J.F. Gallagher, J. Lewis, P.R. Raithby, G.P. Shields, J. Organomet. Chem. 614–615 (2000) 231.
[194] J. Camats, R. Reina, O. Riba, O. Rossell, M. Seco, P. Gómez-Sal, A. Martín, D. De Montauzon, Organometallics 19 (2000) 3316.
[195] C. Femoni, F. Demartin, M.C. Iapalucci, A. Lombardi, G. Longoni, C. Marin, P.H. Svensson, J. Organomet. Chem. 614–615 (2000) 294.
[196] R.D. Adams, J. Organomet. Chem. 600 (2000) 1.
[197] C.E. Housecroft, S.M. Draper, A.D. Hattersley, A.L. Rheingold, J. Organomet. Chem. 614–615 (2000) 202.
[198] T. Chihara, M. Sato, H. Konomoto, S. Kamiguchi, H. Ogawa, Y. Wakatsuki, J. Chem. Soc. Dalton Trans. (2000) 2295.
[199] G. Chiaradonna, G. Ingrosso, F. Marchetti, Angew. Chem. Int. Ed. Engl. 39 (2000) 3872.
[200] T. Nakajima, A. Ishiguro, Y. Wakatsuki, Angew. Chem. Int. Ed. Engl. 39 (2000) 1131.